negative or positive. As shown Fig. 2C, this criterion was actually adaptive for the broad range of rBoPrP concentration.

rBoPrP detection by FCCS in samples prepared from BSE-negative cattle

When we measured the tissue samples prepared from BSE-negative cattle without labeled antibodies as a control experiment, burst signals and high background fluorescence were observed during the time course of fluorescent intensity (data not shown). Because the agents used for preparation had no significant fluorescence in the final concentration, the burst signals and background fluorescence probably were derived from the tissue component but not identified. To improve the detection method using FCCS, therefore, we carried out the detection of rBoPrP in the samples prepared from BSE-negative cattle that mimic the tissue samples containing PrP. Because the structure of PrP denatured from PrP^{Sc} is similar to that of the rBoPrP used, rBoPrP was used as a model experiment and was added to the samples prepared from the BSE-negative cattle after all preparation and separation steps.

Fig. 3A shows FAFs and FCF of mAb72(488) and mAb44B1(647) in PBS (pH 7.3). The FAFs were well fitted with the one-component model. The diffusion times of mAb72(488), mAb44B1(647), and the immune complex mAb72(488)–rBoPrP–mAb44B1(647) were 1.1, 1.2, and 2 ms, respectively. In contrast, unusual FAFs and FCF were obtained in the BSE-negative samples without centrifugation due to burst signals that were assumed to be caused by scattering debris (Fig. 3B).

To overcome this problem, the BSE-negative samples were clarified by centrifugation at 3000*g* for 3 min before FCCS measurement. The FAFs and FCF of centrifuged samples were well fitted with the one-component model (Fig. 3C), where the diffusion times of mAb72(488), mAb44B1(647), and the immune complex were 1.1, 1.3, and 3.5 ms, respectively. There is a difference in the diffusion times of the immune complex in the presence and absence of the BSE-negative samples. Given that the other two faster diffusion times are quite similar, the difference might be caused by low statistical quality of cross-correlation curves [17]. Using ELISA, we confirmed that significant loss of PrP^{Sc} was not observed by centrifugation at 3000*g* for 3 min (Fig. 3D). The value at 0.34 nM rBoPrP remained above the cutoff line when rBoPrP was spiked to the tissue extract from the BSE-negative cattle (Fig. 3E). The detection limit in tissue samples was the same as that in PBS (pH 7.3) (Table 1).

Comparison of FCCS with ELISA for detection limit of rBoPrP and PrP^{Sc}

Although FCCS detected rBoPrP in both PBS (pH 7.3) and the samples prepared from BSE-negative cattle, the apparatus used was too expensive and large to use for BSE diagnosis at abattoirs. Thus, we developed a compact FCCS apparatus. The compact FCCS is small ($200 \times 300 \times 600$ mm) and low cost, and it provides FCF with a high signal-to-noise ratio compared with other systems (data not shown). The sensitivity of the compact FCCS in the detection of rBoPrP and PrP^{Sc} was compared to that of ELISA approved by the European Commission for BSE diagnosis.

Figs. 4A and B show a dose-dependent detection of rBoPrP by FCCS and ELISAs in PBS (pH 7.3) as a simple model of BSE diagnosis. As shown Fig. 4A, the value at 0.24 nM rBoPrP was located above the cutoff line using FCCS in PBS (pH 7.3). This value was nearly the same as that of the Platelia BSE kit (0.15 nM), whereas the FRELISA BSE kit could detect rBoPrP at 0.05 nM in PBS (pH 7.3) (Fig. 4B).

As a more feasible condition of BSE diagnosis, the sensitivity of FCCS was compared with that of ELISAs in the samples prepared from BSE-negative cattle (Figs. 4C and D). The BSE-negative samples were centrifuged at 3000*g* for 3 min to remove scattering debris. The detection limit for rBoPrP using FCCS was 0.15 nM in the BSE-negative samples (Fig. 4C), which was the same as both the Platelia BSE kit (0.15 nM) and FRELISA BSE kit (0.15 nM) (Fig. 4D).

We further compared the sensitivities of FCCS and ELISA using scrapie-affected mice. Only the FRELISA BSE kit was used for the assessment because the antibodies that come with the Platelia BSE kit do not react with mouse PrP^{Sc}. Tissue homogenates from scrapie-affected mice were serially diluted with 4-fold steps in the samples prepared from BSE-negative cattle. Fig. 4E shows a clearly positive change at the 4^{-5}-fold dilution step, and the 4^{-6}-fold dilution step was slightly ahead of the cutoff line in FCCS. In contrast, Fig. 4F shows a clearly positive change at the 4^{-6}-fold dilution in ELISA. The concentration of PrP at the 4^{-6}-fold dilution step was determined by ELISA using rBoPrP (Fig. 4G). The OD value at the 4^{-6}-fold dilution step in Fig. 4F was equal to approximately 0.3 nM rBoPrP. On the other hand, the rBoPrP concentration for FCCS was estimated at approximately 0.13 nM. This is because the samples for FCCS were diluted 2.3-fold compared with those for ELISA (see Materials and methods) to reduce the background signal of the turbid medium and the adverse effect of urea on the immunoreactions. According to the detection limit of FCCS in both PBS (pH 7.3) and the samples prepared from BSE-negative cattle, this estimation was reasonable.

The average detection limits for rBoPrP and PrP^{Sc} using FCS, FCCS, and ELISAs are summarized in Table 1. The FRELISA BSE kit was more sensitive than FCCS in PBS (pH 7.3). FCCS was significantly more sensitive to rBoPrP than FCS in PBS (pH 7.3) and nearly the same as the Platelia BSE kit in the three experimental conditions.

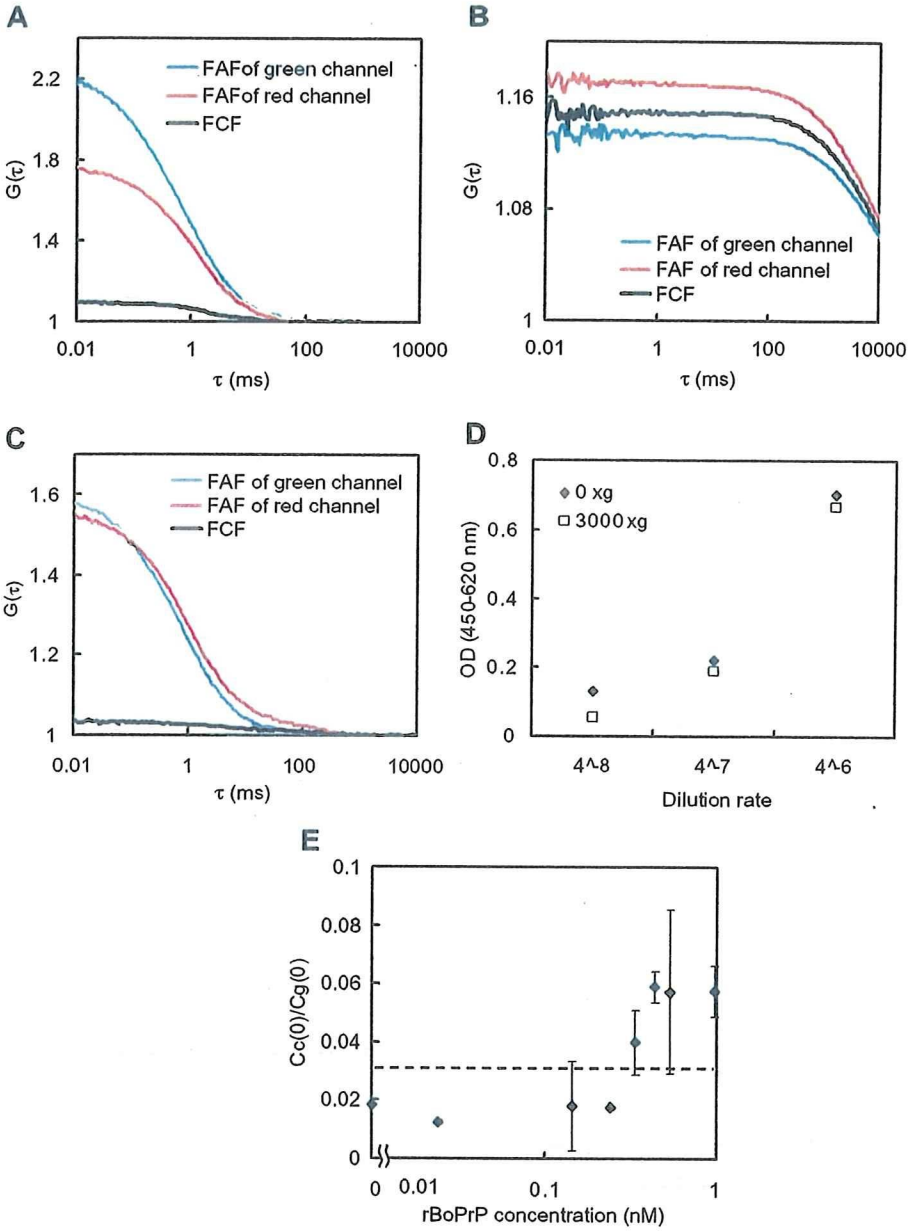

Fig. 3. rBoPrP detection by FCCS in samples prepared from BSE-negative cattle. (A–C) FAFs and FCF of the immune complex mAb72(488)–rBoPrP–mAb44B1(647) in PBS (pH 7.3) (A), in the BSE-negative samples without centrifugation (B), and in the BSE-negative samples with centrifugation at 3000*g* for 3 min. FAFs of green and red channels were derived from mAb72(488) and mAb44B1(647), respectively. The concentrations of mAb72(488), mAb44B1(647), and rBoPrP used were 0.5, 0.5, and 0.97 nM, respectively. (D) Effect of centrifugation on detection of PrP^{Sc} from infected mice. (E) Detection limit for rBoPrP using FCCS in BSE-negative samples. The concentrations of mAb72(488) and mAb44B1(647) used were 0.7 and 0.6 nM, respectively. The broken line indicates the cutoff value. Data are expressed as means ± standard deviations. (For interpretation of the references to color in this figure legend, the reader is referred to the Web version of this article.)

Discussion

Most of the diagnostic tests for TSEs are based on the detection of PrP^{Sc} using appropriate PrP-specific antibodies after the removal of cellular PrP from samples by treatment with proteinase K (PK) [29]. Although Western blotting is a widely validated method for PrP^{Sc} detection, its disadvantages as a screening test are that only a few samples can be processed in a single gel and that it is time-consuming and requires experienced personnel. Some of these limitations have been overcome by using ELISA for PrP^{Sc} detection [30,31]. Several spectrophotometric techniques, such as Fourier transformed infrared spectroscopy [32], multispectral UV fluoroscopy [33], and fluores-

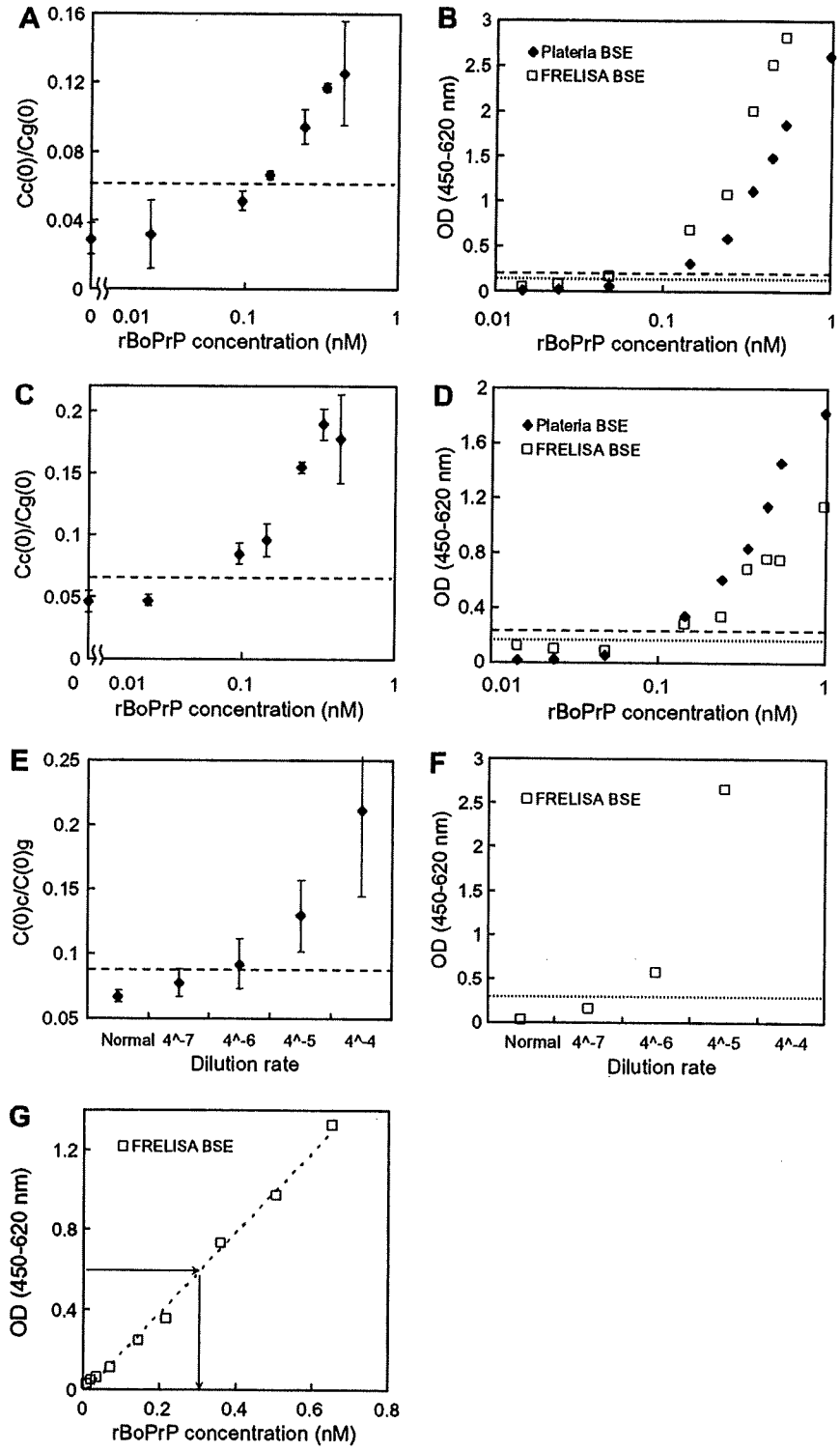

Fig. 4. Comparison of FCCS with ELISA for detection limit of rBoPrP and PrP^{Sc}. (A,C) rBoPrP detection using compact FCCS in PBS (pH 7.3) (A) and in the BSE-negative samples (C). (E) PrP^{Sc} detection from infected mice. The concentrations of mAb72(488) and mAb44B1(647) used were 0.1 and 0.1 nM, respectively. Normal on the x axis means the samples prepared from BSE-negative cattle. The broken line indicates the cutoff value determined from the mean of non-rBoPrP samples plus 3 standard deviations. Data are expressed as means ± standard deviations. (B,D) rBoPrP detection using a Platelia BSE kit and a FRELISA BSE kit in PBS (pH 7.3) (B) and in the BSE-negative samples (D). (F) PrP^{Sc} detection from infected mice. Normal on the x axis means the samples prepared from BSE-negative cattle. The broken and dotted lines indicate the cutoff values of the Platelia BSE kit and the FRELISA BSE kit, respectively. (G) OD value versus rBoPrP concentration in FRELISA BSE kit. The arrow indicates the concentration of rBoPrP at the OD value of the 4^{-6}-fold dilution step in panel F.

cence detection after capillary electrophoresis [34], are also being developed as sensitive methods for detection of PrP^{Sc}.

Bieschke and coworkers [35] developed a highly sensitive detection method based on a two-color scanning setup, where intensity analysis is used to detect pathological aggregates of PrP^{Sc} having slow diffusion instead of correlating signals to get size information on the molecule. However, equipment where the samples need to be moved to the focal area by scanning stage seems to be too expensive and sophisticated to use for BSE diagnosis at abattoirs. In this study, we have developed methods for the detection of PrP using conventional FCS and FCCS analyses and attempted to detect PrP^{Sc} using the compact FCCS system produced with the aim of BSE diagnosis at abattoirs.

Although antibodies are essential tools for immunological diagnosis, there are limitations in their use for FCS. Mayboroda and coworkers [36] showed that staphylococcal protein A (PrA, 42 kDa) can be used as a low-molecular weight tag for immune complex. However, PrA is applied not for mouse IgG_1 but for IgG_{2a}, IgG_{2b}, and IgG_3 [37]. Actually, we could not detect rBoPrP with PrA using FCS because there was no difference between the affinity of PrA for immune complexes and that for free anti-PrP antibodies 72 and 44B1. On the other hand, the use of both Fab′ fragment and another antibody binding to independent epitopes is generally applicable for the detection of every antigen using FCS.

Unlike FCS analysis, depending on diffusion time, FCCS is not necessary to prepare a lower molecular weight probe, such as a labeled Fab′ fragment, or to determine the difference of the solution's viscosity for each sample, but the dynamic range of FCCS in this experiment was narrower than that of FCS. This is because nearly identical concentrations of two mAbs labeled with different fluorescence dyes were used in FCCS due to suppression of background fluorescence, whereas sufficient unlabeled antibody was used in FCS to form 44B1–rBoPrP completely. To overcome the limitation of dynamic range, another measurement was carried out with the addition of rBoPrP to all of the samples; namely, by comparing measurements without and with the addition of 4.8 nM rBoPrP, we can determine whether the sample is negative or positive. This technique is generally applicable for other sandwich detection methods with two probes. However, because all samples would need to be measured at least twice given that the majority of all samples in BSE diagnosis are expected to be negative, the problem remains the key issue for the diagnosis using FCCS. The reduction of measuring time in a sample and the development of a totally automated system might be a solution to the problem.

Although the detection and characterization of prion disease [35,38], Alzheimer's disease [39], and Parkinson's disease [40] were reported using confocal fluorescence methods, they were restricted to analyses in transparent media such as reaction buffer and cerebrospinal fluid (CSF). In contrast, we detected PrP using FCCS in turbid samples prepared from tissue. Because the use of both centrifugation and sufficiently labeled antibodies is easy, they are generally applicable for the detection of the target molecule using FCCS in turbid medium.

From infectivity studies in rodent models of TSE [41], it seems that the maximum concentration of infectivity in circulating blood resides in the buffy coat, where the concentration ranges between 5 to 10 infectious units (IU) ml^{-1} and approximately 100 IU ml^{-1} at the onset of symptomatic disease. One picogram of PrP^{Sc} is estimated to contain 100 IU [42]; therefore, the concentrations of PrP^{Sc} in the buffy coat are expected to be 1 pg ml^{-1} (33 fM) and 0.1 pg ml^{-1} (3.3 fM) during the symptomatic and presymptomatic phases, respectively.

In the femtomolar concentration range, a target molecule has a territory of 1 nl, whereas the confocal volume of FCS or FCCS is approximately 1 fl. If the radius of the confocal volume and the diffusion coefficient of particles are 1 μm and 10^{-6} cm^2/s, respectively, the femtomolar concentration is detectable for 15 min measurement using FCS and FCCS [16]. Because this calculation assumes that all of the PrP binds to the fluorescent-labeled antibody, the sensitivity seems to be strongly limited by the K_d values of antibodies. Therefore, high-affinity antibodies to PrP are required for the development of a highly sensitive detection method.

Castilla and coworkers [43] developed an efficient protocol for the amplification of PrP^{Sc}. The combination of our detection method and amplification technique of PrP^{Sc} can improve the detection limit of PrP^{Sc}. A perfect and stable overlap of two laser lines often is difficult, and this makes the reduction of FCF amplitude and sensitivity. Thus, we currently are developing a novel detection method for sensitive improvement with new dyes in FCCS analysis.

All commercial BSE tests currently used detect the PK resistance of PrP, but it has been reported that the pathological state of PrP was not only PK resistant but also PK sensitive [44]. Birkmann and coworkers [45,46] developed methods for detecting both parts of the prion particles with FCS in fluorescence intensity distribution analysis (FIDA) mode, although the limit of sensitivity has not been exploited. On the other hand, our methods demonstrated that denatured PrP and rBoPrP are suitable for the detection of only the PK-resistant form. In the future, the methods need to improve to detect the entire pathological state of PrP.

In conclusion, we have presented methods for the detection of PrP using FCS and FCCS. A combination of a fluorescent-labeled Fab′ fragment and another anti-PrP mAb enabled us to detect rBoPrP using FCS. On the other hand, FCCS detected rBoPrP using two mAbs labeled with different fluorescence dyes. The sensitivity of a compact FCCS apparatus produced with the aim of BSE diagnosis at abattoirs was comparable to that of the ELISA approved by the European Commission for BSE diagnosis. Because

FCS and FCCS analyses require only microliter samples and a single mixing step, the analyses lend themselves to automation for BSE diagnosis.

Acknowledgments

We thank Yutaka Hasegawa, Masami Sugie, Hisayuki Matsui, and Hideki Shimoi (Hamamatsu Photonics) for the construction of the compact FCCS apparatus and cooperative technical assistance; Takayuki Yanagiya and Jun-ichi Azumi (Fujirebio) for the gift of anti-PrP antibodies and rBoPrP as well as cooperative discussions; Yoshifumi Yamada and Olympus for technical assistance; and Kenta Saito and Kanji Sato for valuable comments. This work was supported by the Japan Science and Technology Agency and in part by a Health and Labor Sciences Research Grants for research on food safety from the Ministry of Health, Labor, and Welfare of Japan.

References

[1] S.B. Prusiner, Prions, Proc. Natl. Acad. Sci. USA 95 (1998) 13363–13383.
[2] R.G. Will, J.W. Ironside, M. Zeidler, S.N. Cousens, K. Estibeiro, A. Alperovitch, S. Poser, M. Pocchiari, A. Hofman, P.G. Smith, A new variant of Creutzfeldt–Jakob disease in the UK, Lancet 347 (1996) 921–925.
[3] C.A. Llewelyn, P.E. Hewitt, R.S. Knight, K. Amar, S. Cousens, J. Mackenzie, R.G. Will, Possible transmission of variant Creutzfeldt–Jakob disease by blood transfusion, Lancet 363 (2004) 417–421.
[4] A.H. Peden, M.W. Head, D.L. Ritchie, J.E. Bell, J.W. Ironside, Preclinical vCJD after blood transfusion in a PRNP codon 129 heterozygous patient, Lancet 364 (2004) 527–529.
[5] D. Magde, E.L. Elson, W.W. Webb, Fluorescence correlation spectroscopy: I. Conceptual basis and theory, Biopolymers 13 (1974) 1–27.
[6] R. Rigler, U. Mets, J. Widengren, P. Kask, Fluorescence correlation spectroscopy with high count rates and low background analysis of translational diffusion, Eur. Biophys. J. 22 (1993) 169–175.
[7] M. Kinjo, R. Rigler, Ultrasensitive hybridization analysis using fluorescence correlation spectroscopy, Nucleic Acids Res. 23 (1995) 1795–1799.
[8] C.G. Pack, G. Nishimura, M. Tamura, K. Aoki, H. Taguchi, M. Yoshida, M. Kinjo, Analysis of interaction between chaperonin GroEL and its substrate using fluorescence correlation spectroscopy, Cytometry 36 (1999) 247–253.
[9] C.G. Pack, K. Aoki, H. Taguchi, M. Yoshida, M. Kinjo, M. Tamura, Effect of electrostatic interactions on the binding of charged substrate to GroEL studied by highly sensitive fluorescence correlation spectroscopy, Biochem. Biophys. Res. Commun. 267 (2000) 300–304.
[10] R. Rigler, E.L. Elson (Eds.), Fluorescence Correlation Spectroscopy: Theory and Applications, Springer, Berlin, 2001.
[11] A. Kitamura, H. Kubota, C. Pack, G. Matsumoto, S. Hirayama, Y. Takahashi, H. Kimura, M. Kinjo, R. Morimoto, K. Nagata, Cytosolic chaperonin prevents polyglutamine toxicity with altering the aggregation state, Nat. Cell Biol. 10 (2006) 1163–1170.
[12] N. Yoshida, M. Kinjo, M. Tamura, Microenvironment of endosomal aqueous phase investigated by the mobility of microparticles using fluorescence correlation spectroscopy, Biochem. Biophys. Res. Commun. 280 (2001) 312–318.
[13] K. Saito, E. Ito, Y. Takakuwa, M. Tamura, M. Kinjo, In situ observation of mobility and anchoring of PKC(I in plasma membrane, FEBS Lett. 541 (2003) 126–131.
[14] C. Pack, K. Saito, M. Tamura, M. Kinjo, Microenvironment and effect of energy depletion in the nucleus analyzed by mobility of multiple oligomeric EGFPs, Biophys. J. 10 (2006) 3921–3936.
[15] K.M. Berland, Detection of specific DNA sequences using dual-color two-photon fluorescence correlation spectroscopy, J. Biotechnol. 108 (2004) 127–136.
[16] M. Eigen, R. Rigler, Sorting single molecules: Application to diagnostics and evolutionary biotechnology, Proc. Natl. Acad. Sci. USA 91 (1994) 5740–5747.
[17] P. Schwille, F.J. Meyer-Almes, R. Rigler, Dual-color fluorescence cross-correlation spectroscopy for multicomponent diffusional analysis in solution, Biophys. J. 72 (1997) 1878–1886.
[18] T. Kohl, K.G. Heinze, R. Kuhlemann, A. Koltermann, P. Schwille, A protease assay for two-photon cross-correlation and FRET analysis based solely on fluorescent proteins, Proc. Natl. Acad. Sci. USA 99 (2002) 12161–12166.
[19] T. Takagi, H. Kii, M. Kinjo, DNA measurements by using fluorescence correlation spectroscopy and two-color fluorescence cross correlation spectroscopy, Curr. Pharm. Biotechnol. 5 (2004) 199–204.
[20] Z. Foldes-Papp, M. Kinjo, M. Tamura, E. Birch-Hirschfeld, U. Demel, G.P. Tilz, A new ultrasensitive way to circumvent PCR-based allele distinction: Direct probing of unamplified genomic DNA by solution-phase hybridization using two-color fluorescence cross-correlation spectroscopy, Exp. Mol. Pathol. 78 (2005) 177–189.
[21] K. Saito, I. Wada, M. Tamura, M. Kinjo, Direct detection of caspase-3 activation in single live cells by cross-correlation analysis, Biochem. Biophys. Res. Commun. 324 (2004) 849–854.
[22] T. Kohl, E. Haustein, P. Schwille, Determining protease activity *in vivo* by fluorescence cross-correlation analysis, Biophys. J. 89 (2005) 2770–2782.
[23] T. Kogure, S. Karasawa, T. Araki, K. Saito, M. Kinjo, A. Miyawaki, Dual-color fluorescence cross-correlation spectroscopy using a fluorescent protein with a large Stokes shift, Nat. Biotechnol. 5 (2006) 577–581.
[24] O. Stoevesandt, K. Kohler, R. Fischer, I.C. Johnston, R. Brock, One-step analysis of protein complexes in microliters of cell lysate, Nat. Methods 2 (2005) 833–835.
[25] M. Shinagawa, K. Takahashi, S. Sasaki, S. Doi, H. Goto, G. Sato, Characterization of scrapie agent isolated from sheep in Japan, Microbiol. Immunol. 29 (1985) 543–551.
[26] C.L. Kim, A. Umetani, T. Matsui, N. Ishiguro, M. Shinagawa, M. Horiuchi, Antigenic characterization of an abnormal isoform of prion protein using a new diverse panel of monoclonal antibodies, Virology 320 (2004) 40–51.
[27] S. Yoshitake, M. Imagawa, E. Ishikawa, Y. Niitsu, I. Urushizaki, M. Nishiura, R. Kanazawa, H. Kurosaki, S. Tachibana, N. Nakazawa, H. Ogawa, Mild and efficient conjugation of rabbit Fab′ and horseradish peroxidase using a maleimide compound and its use for enzyme immunoassay, J. Biochem. (Tokyo) 92 (1982) 1413–1424.
[28] U. Meseth, T. Wohland, R. Rigler, H. Vogel, Resolution of fluorescence correlation measurements, Biophys. J. 76 (1999) 1619–1631.
[29] D.C. Bolton, M.P. McKinley, S.B. Prusiner, Identification of a protein that purifies with the scrapie prion, Science 218 (1982) 1309–1311.
[30] K.U. Grathwohl, M. Horiuchi, N. Ishiguro, M. Shinagawa, Sensitive enzyme-linked immunosorbent assay for detection of PrP^{Sc} in crude tissue extracts from scrapie-affected mice, J. Virol. Methods 64 (1997) 205–216.
[31] J.P. Deslys, E. Comoy, S. Hawkins, S. Simon, H. Schimmel, G. Wells, J. Grassi, J. Moynagh, Screening slaughtered cattle for BSE, Nature 409 (2001) 476–478.
[32] P. Lasch, J. Schmitt, M. Beekes, T. Udelhoven, M. Eiden, H. Fabian, W. Petrich, D. Naumann, Antemortem identification of bovine spongiform encephalopathy from serum using infrared spectroscopy, Anal. Chem. 75 (2003) 6673–6678.
[33] R. Rubenstein, P.C. Gray, C.M. Wehlburg, J.S. Wagner, G.C. Tisone, Detection and discrimination of PrP^{Sc} by multi-spectral

ultraviolet fluorescence, Biochem. Biophys. Res. Commun. 246 (1998) 100–106.
[34] M.J. Schmerr, A.L. Jenny, M.S. Bulgin, J.M. Miller, A.N. Hamir, R.C. Cutlip, K.R. Goodwin, Use of capillary electrophoresis and fluorescent labeled peptides to detect the abnormal prion protein in the blood of animals that are infected with a transmissible spongiform encephalopathy, J. Chromatogr. 853 (1999) 207–214.
[35] J. Bieschke, A. Giese, W. Schulz-Schaeffer, I. Zerr, S. Poser, M. Eigen, H. Kretzschmar, Ultrasensitive detection of pathological prion protein aggregates by dual-color scanning for intensely fluorescent targets, Proc. Natl. Acad. Sci. USA 97 (2000) 5468–5473.
[36] O.A. Mayboroda, A. van Remoortere, H.J. Tanke, C.H. Hokke, A.M. Deelder, A new approach for fluorescence correlation spectroscopy (FCS) based immunoassays, J. Biotechnol. 107 (2004) 185–192.
[37] J.J. Langone, Immune complex formation enhances the binding of staphylococcal protein A to immunoglobulin G, Biochem. Biophys. Res. Commun. 30 (1980) 473–479.
[38] J. Levin, U. Bertsch, H. Kretzschmar, A. Giese, Single particle analysis of manganese-induced prion protein aggregates, Biochem. Biophys. Res. Commun. 329 (2005) 1200–1207.
[39] M. Pitschke, R. Prior, M. Haupt, D. Riesner, Detection of single amyloid β-protein aggregates in the cerebrospinal fluid of Alzheimer's patients by fluorescence correlation spectroscopy, Nat. Med. 4 (1998) 832–834.
[40] A. Giese, B. Bader, J. Bieschke, G. Schaffar, S. Odoy, P.J. Kahle, C. Haass, H. Kretzschmar, Single particle detection and characterization of synuclein co-aggregation, Biochem. Biophys. Res. Commun. 333 (2005) 1202–1210.
[41] P. Brown, R.G. Rohwer, B.C. Dunstan, C. MacAuley, D.C. Gajdusek, W.N. Drohan, The distribution of infectivity in blood components and plasma derivatives in experimental models of transmissible spongiform encephalopathy, Transfusion 38 (1998) 810–816.
[42] P. Brown, L. Cervenakova, H. Diringer, Blood infectivity and the prospects for a diagnostic screening test in Creutzfeldt–Jakob disease, J. Lab. Clin. Med. 137 (2001) 5–13.
[43] J. Castilla, P. Saa, C. Soto, Detection of prions in blood, Nat. Med. 11 (2005) 982–985.
[44] J. Safar, H. Wille, V. Itri, D. Groth, H. Serban, M. Torchia, F.E. Cohen, S.B. Prusiner, Eight prion strains have PrP^{Sc} molecules with different conformations, Nat. Med. 10 (1998) 1157–1165.
[45] E. Birkmann, O. Schafer, N. Weinmann, C. Dumpitak, M. Beekes, R. Jackman, L. Thorne, D. Riesner, Detection of prion particles in samples of BSE and scrapie by fluorescence correlation spectroscopy without proteinase K digestion, Biol. Chem. 387 (2006) 95–102.
[46] E. Birkmann, F. Henke, N. Weinmann, C. Dumpitak, M. Groschup, A. Funke, D. Willbold, D. Riesner, Counting of single prion particles bound to a capture-antibody surface (surface-FIDA), Vet. Microbiol. 16 (2007) 226–229.

Immunology
The Journal of cells, molecules, systems and technologies
British Society for immunology

IMMUNOLOGY ORIGINAL ARTICLE

Alteration of *N*-glycosylation in the kidney in a mouse model of systemic lupus erythematosus: relative quantification of *N*-glycans using an isotope-tagging method

Noritaka Hashii,[1,2] Nana Kawasaki,[1,2] Satsuki Itoh,[1] Yukari Nakajima,[1,2] Toru Kawanishi[1] and Teruhide Yamaguchi[1]

[1]*Division of Biological Chemistry and Biologicals, National Institute of Health Sciences, Setagaya-ku, Tokyo, Japan, and* [2]*Core Research for Evolutional Science and Technology (CREST) of the Japan Science and Technology Agency (JST), Kawaguchi City, Saitama, Japan*

doi:10.1111/j.1365-2567.2008.02898.x
Received 19 March 2008; revised 28 May 2008; accepted 2 June 2008.
Correspondence: N. Kawasaki, Division of Biological Chemistry and Biologicals, National Institute of Health Sciences, 1-18-1 Kamiyouga, Setagaya-ku, Tokyo 158-8501, Japan. Email: nana@nihs.go.jp
Senior author: Teruhide Yamaguchi, email: yamaguch@nihs.go.jp

Summary

Changes in the glycan structures of some glycoproteins have been observed in autoimmune diseases such as systemic lupus erythematosus (SLE) and rheumatoid arthritis. A deficiency of α-mannosidase II, which is associated with branching in *N*-glycans, has been found to induce SLE-like glomerular nephritis in a mouse model. These findings suggest that the alteration of the glycosylation has some link with the development of SLE. An analysis of glycan alteration in the disordered tissues in SLE may lead to the development of improved diagnostic methods and may help to clarify the carbohydrate-related pathogenic mechanism of inflammation in SLE. In this study, a comprehensive and differential analysis of *N*-glycans in kidneys from SLE-model mice and control mice was performed by using the quantitative glycan profiling method that we have developed previously. In this method, a mixture of deuterium-labelled *N*-glycans from the kidneys of SLE-model mice and non-labelled *N*-glycans from kidneys of control mice was analysed by liquid chromatography/mass spectrometry. It was revealed that the low-molecular-mass glycans with simple structures, including agalactobiantennary and paucimannose-type oligosaccharides, markedly increased in the SLE-model mouse. On the other hand, fucosylated and galactosylated complex type glycans with high branching were decreased in the SLE-model mouse. These results suggest that the changes occurring in the *N*-glycan synthesis pathway may cause the aberrant glycosylations on not only specific glycoproteins but also on most of the glycoproteins in the SLE-model mouse. The changes in glycosylation might be involved in autoimmune pathogenesis in the model mouse kidney.

Keywords: isotope-tagging method; liquid chromatography/multiple-stage mass spectrometry; systemic lupus erythematosus

Introduction

Glycosylation is one of the most common post-translational modifications[1,2] and contributes to many biological processes, including protein folding, secretion, embryonic development and cell–cell interactions.[3] Alteration of glycosylation is associated with several diseases, including inflammatory responses and malignancies;[4–6] for instance, significant increases in fucosylation and branching are found in ovarian cancer and lung cancer.[7] Additionally, the carbohydrate structure changes from type I glycans (Galβ1-3GlaNAc) to type II glycans (Galβ1-4GalNAc) in carcinoembryonic antigen in colon cancer.[8] Furthermore, an increase in biantennary oligosaccharides lacking galactose (Gal) was found on immunoglobulin G (IgG) in systemic lupus erythematosus (SLE) and rheumatoid arthritis,[9–11] and agalactoglycans are used for the early diagnosis of rheumatoid arthritis.[12]

Systemic lupus erythematosus is an autoimmune disease characterized as chronic and as a systemic disease, with symptoms such as kidney failure, arthritis and erythema. In addition to the known changes in glycosylation on IgG, there have been several reports on the association between glycosylation and inflammation in SLE and rheumatoid

arthritis.[13–15] A deficiency of α-mannosidase II (αM-II), which is associated with branching in *N*-glycans, has been found to induce human SLE-like glomerular nephritis in a mouse model.[16] Green *et al.* reported that branching structures of *N*-glycan in mammals are involved in protection against immune responses in autoimmune disease pathogenesis.[17] Although there is no direct evidence that alteration of glycosylation is the upstream event in the pathogenesis of SLE, these findings suggest that changes in the glycan structure may be involved in the inflammatory-related autoimmune disorder. Glycosylation analysis may lead to the development of improved diagnostic methods and may help to clarify the carbohydrate-related pathogenic mechanism of inflammation in SLE.

Mass spectrometry (MS) and liquid chromatography/mass spectrometry (LC/MS) are the most prevalent strategies for identifying disease-related glycans in glycomics.[18–20] Aberrant glycosylations in some disease samples have been found by comparing mass spectra or chromatograms between normal and disease samples; however, because of the tremendous heterogeneities of the sugar moiety in glycoprotein as well as the low reproducibility of LC/MS, accurate quantitative analysis is difficult using MS and LC/MS alone. To overcome these problems, we previously developed the stable isotope-tagging method for the quantitative profiling of glycans using 2-aminopyridine (AP).[21] After the glycans are released from sample and the reference glycoproteins are derivatized to pyridyl amino (d_0-PA) glycans and to tetra-deuterium-labelled pyridyl amino (d_4-PA) glycans, respectively, a mixture of both d_0-PA and d_4-PA glycans was subjected to LC/MS, and the levels of individual glycans were calculated from the intensity ratios of d_0-glycan and d_4-glycan molecular ions (Fig. 1a). Recently, alternative isotope-tagging methods using deuterium-labelled compounds, such as 2-aminobenzoic acid its derivatives, and permethylation, have been proposed by other groups.[22–24] All of these studies prove the utility of isotope-tagging methods for the quantitative analysis of glycosylation.

In the present study, we used the isotope-tagging method to analyse changes in *N*-glycosylation in the disordered kidney in an SLE mouse model. We used an MRL/MpJ-lpr/lpr (MRL-lpr) mouse which lacks the Fas antigen gene.[25–27] The MRL-lpr mouse is known to naturally develop SLE-like glomerular nephritis and is widely used in SLE studies. MRL/MpJ-+/+ (MRL-+/+) mice were used as controls.

Materials and methods

Materials

The kidneys of the SLE-model mice (MRL-lpr) and control mice (MRL-+/+) (n = 3) were purchased from Japan SLC, Inc. (Hamamatsu, Japan). Thermolysin (EC 3.4.24.27), originating from *Bacillus thermoproteolyticus*

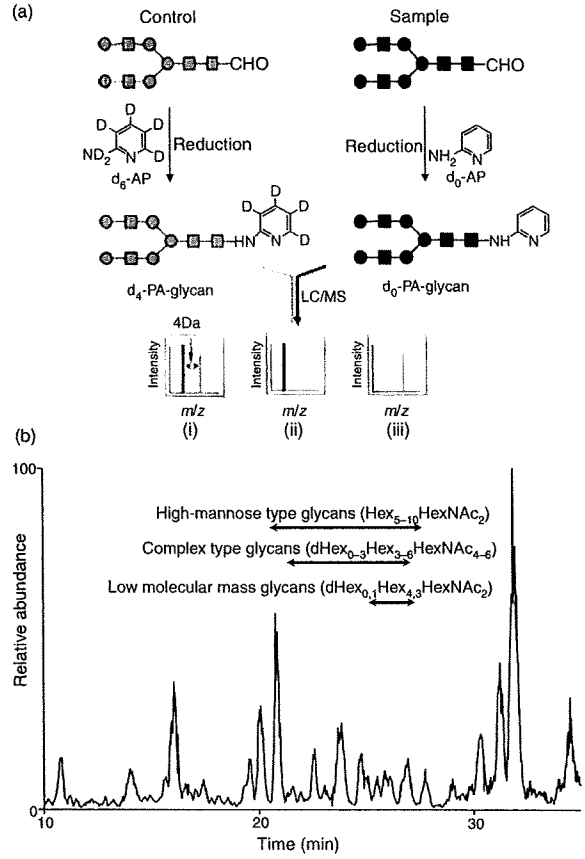

Figure 1. (a) Quantitative glycan profiling using the stable isotope-tagging method and liquid chromatography/mass spectrometry (LC/MS). (i) sample = control, (ii) sample > control, (iii) sample < control. (b) Total ion chromatogram obtained by a single scan (m/z 700–2000) of the d_0-glycan and d_4-glycan mixture.

Rokko, was purchased from Daiwa Kasei (Shiga, Japan). Glycopeptidase A (PNGase A) was obtained from Seikagaku Kogyo Corporation (Tokyo, Japan). Non-deuterium-labelled 2-aminopyridine (d_0-AP) and deuterium-labelled 2-aminopyridine (d_6-AP) were purchased from Takara Bio (Otsu, Japan) and Cambridge Isotope Laboratories (Andover, MA), respectively.

Sample preparation

Mouse kidneys were filtered using a cell strainer (70 μm; BD Biosciences, San Jose, CA) and contaminating blood cells in the kidney cells were burst in 140 mM NH_4Cl–Tris buffer (pH 7·2). The surviving kidney cells were washed three times with phosphate-buffered saline containing a mixture of protease inhibitors (Wako, Tokyo, Japan) and dissolved in guanidine–HCl buffer (8 M guanidine–HCl, 0·5 M Tris–HCl, pH 8·6) containing a mixture of protease inhibitors by vortexing at 4°. The protein concentration was measured using a 2-D Quant Kit (GE Healthcare

Bio-Sciences, Uppsala, Sweden). The protein solution (200 μg proteins) was incubated with 40 mM dithiothreitol at 65° for 30 min. Freshly prepared sodium iodoacetate (final concentration, 96 mM) was added to the sample solution, and the mixture was incubated at room temperature for 40 min in the dark. The reaction was stopped by adding cystine (6 mg/ml in 2 M HCl) in an amount equal to the amount of dithiothreitol. The solution containing carboxymethylated proteins was diluted in four times its volume of H_2O, and the mixture was incubated with 0·1 μg of thermolysin at 65° for 1 hr. After terminating the reaction by boiling, the reaction mixture was diluted in four times its volume of 0·2 M acetate buffer. The *N*-linked glycans were released by treatment with PNGase A (1 mU) at 37° for 16 hr and were desalted using an EnviCarb C cartridge (Supelco, Bellefonte, PA).

Labelling of N-glycans with d_0-AP and d_6-AP

Glycans released from the SLE-model mouse cells were incubated in acetic acid (20 μl) with 12·5 M d_0-AP at 90° for 1 hr. Next, 3·3 M borane–dimethylamine complex reducing reagent in acetic acid (20 μl) was added to the solution and the mixture was incubated at 80° for 1 hr. Excess reagent was removed by evaporation, and d_0-PA glycans were desalted using an EnviCarb C cartridge, concentrated in a SpeedVac and reconstituted in 20 μl of 5 mM ammonium acetate (pH 9·6). Glycans released from the control mouse were labelled with d_6-AP in a similar manner. The resulting d_4-PA glycans were combined with d_0-PA glycans, which were prepared from an equal amount of proteins.

On-line liquid chromatography/mass spectrometry

The sample solution (4 μl) was injected into the LC/MS system through a 5-μl capillary loop. The d_0-PA and d_4-PA glycans were separated in a graphitized carbon column (Hypercarb, 150 × 0·2 mm, 5 μm; Thermo Fisher Scientific, Waltham, MA) at a flow rate of 2 μl/min in a Magic 2002 LC system (Michrom Bioresources, Auburn, CA). The mobile phases were 5 mM ammonium acetate containing 2% acetonitrile (pH 9·6, A buffer) and 5 mM ammonium acetate containing 90% acetonitrile (pH 9·6, B buffer). The PA-glycans were eluted with a linear gradient of 5–45% of B buffer for 90 min.

Mass spectrometric analysis of PA glycans was performed using a Fourier transform ion cyclotron resonance/ion trap mass spectrometer (FT-ICR-MS, LTQ-FT; Thermo Fisher Scientific) equipped with a nanoelectrospray ion source (AMR, Tokyo, Japan). For MS, the electrospray voltage was 2·0 kV in the positive ion mode, the capillary temperature was 200°, the collision energy was 25% for MS^n experiment, and the maximum injection times for FT-ICR-MS and MS^n were 1250 and 50 milliseconds, respectively. The resolution of FT-ICR-MS was 50 000, the scan time (*m/z* 700–2000) was approximately 0·2 seconds, dynamic exclusion was 18 seconds, and the isolation width was 3·0 U (range of precursor ions ± 1·5).

Results

Quantitative profiling of kidney oligosaccharides in the SLE-model mouse

The recovery of oligosaccharides from whole tissues and cells is generally low because of the insolubility of the membrane fraction and possible degradation of the glycans. To improve the recovery of *N*-glycans from kidney cells, whole cells were dissolved in guanidine hydrochloride solution, and all proteins, including membrane proteins, were digested into peptides and glycopeptides with thermolysin. The *N*-glycans were then released from the glycopeptides with PNGase A, which is capable of liberating *N*-linked oligosaccharides even at the N- and/or C-terminals of peptides. The *N*-linked oligosaccharides from the SLE-model mice and control mice were labelled with d_0-AP and d_6-AP, respectively. The mixture of labelled glycans derived from an equal amount of proteins was subjected to quantitative glycan profiling using LC/MS^n.

Figure 1(b) shows the total ion chromatogram obtained by a single mass scan (*m/z* 700–2000) of the glycan mixture in the positive ion mode. Although the MS data contain many MS spectra derived from contaminating low-molecular-weight peptides, the MS/MS spectra of oligosaccharides could be sorted based on the existence of carbohydrate-distinctive ions, such as $HexHexNAc^+$ (*m/z* 366) and $Hex(dHex)HexNAc^+$ (*m/z* 512). The monosaccharide compositions of the precursor ions were calculated from accurate *m/z* values acquired by FT-ICR-MS. Oligosaccharides found at 25–27 min were assigned to low-molecular-mass glycans consisting of $dHex_{0,1}Hex_{4,3}HexNAc_2$ (dHex, deoxyhexose; Hex, hexose; HexNAc, *N*-acetylhexosamine). High-mannose-type glycans, which consist of $Hex_{5-10}HexNAc_2$, were located at 20–28 min; complex-type glycans ($dHex_{0-3}Hex_{3-6}HexNAc_{4-6}$) were found at 21–27 min. Figure 2(a) shows the relative intensities of the molecular ions of *N*-glycans in the SLE-model mouse, which may correspond roughly to the levels of individual *N*-glycans. More than half of all glycans were complex-type oligosaccharides, and the most prominent glycan was $dHex_3Hex_5HexNAc_5$. Man-9 ($Hex_9HexNAc_2$) was the second most common oligosaccharide. Nearly one-quarter of the glycans were low-molecular-mass glycans, and $dHex_1Hex_2HexNAc_2$ was the third most abundant glycan in the SLE-model mouse. The rate of percentage change in individual glycans between the SLE-model mice and control mice was calculated from the intensity ratio of d_0-glycan and d_4-glycan

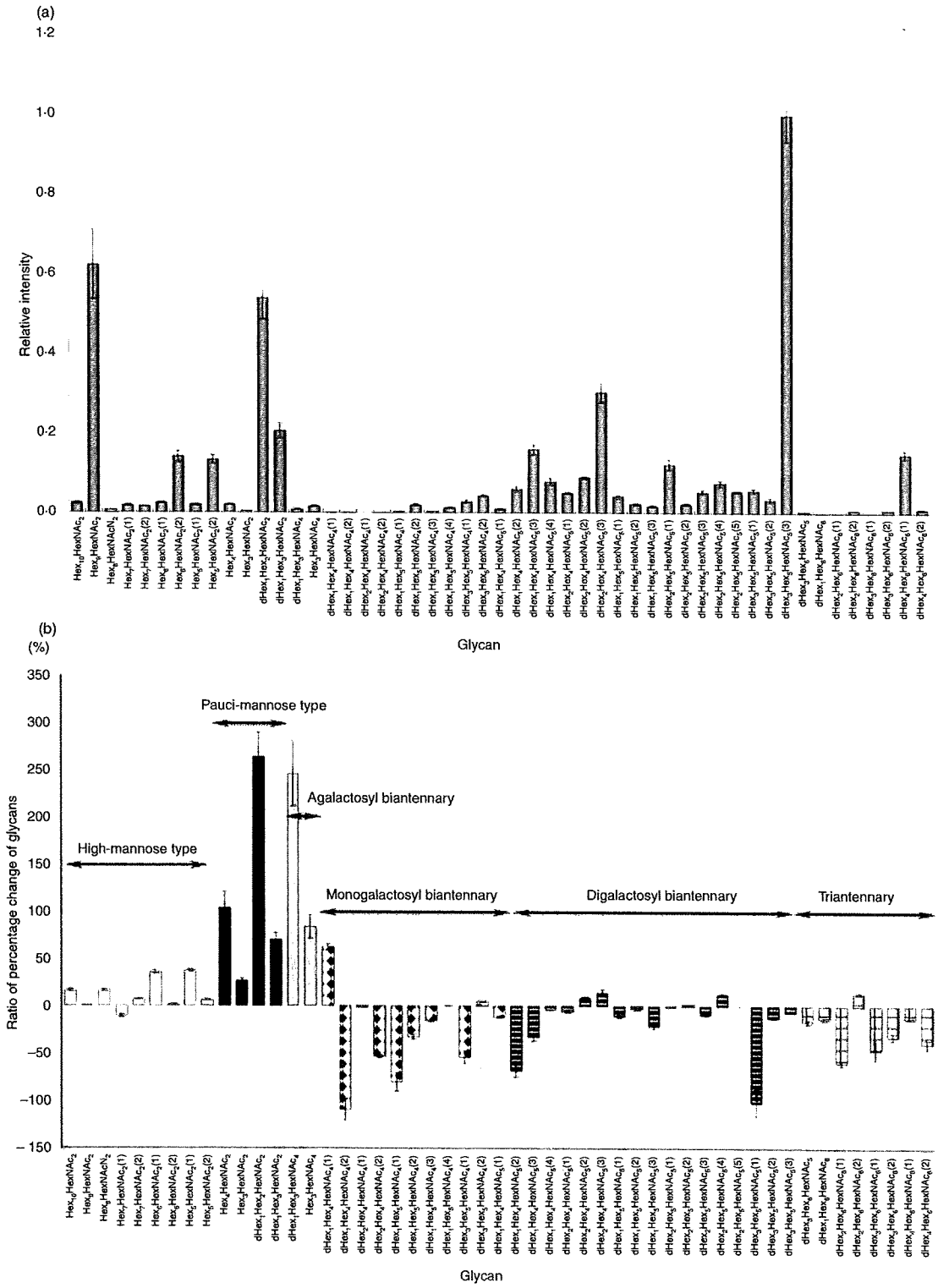

Figure 2. (a) Relative intensities of the molecular ions of d_0-pyridyl amino (PA) glycans from the systemic lupus erythematosus (SLE) model mouse. The intensity of the most intense ion ($[M + 2H]^{2+}$of d_4-PA $dHex_3Hex_5HexNAc_3(3)$, *m/z* 1180·97) was taken as 1·0. (b) Rate of percentage change of d_0/d_4-glycans. Each value is the average of three biological repeats. Error bars correspond to the standard deviation. The numbers in parentheses show the isomers.

molecular ions (Fig. 2b). The significant changes found in many glycans are described below.

Increased oligosaccharides in the SLE-model mouse

Figure 3(a,b) show the mass and MS/MS spectra of the most increased glycan, which showed a notable increase in the SLE-model mouse. Based on *m/z* values of molecular ions and differences of 1·00 U in *m/z* values among monoisotopic ions, the intense ion (*m/z* 973·40) and its neighbour ion (*m/z* 977·43) were assigned to $[M+H]^+$ of d_0-PA $dHex_1Hex_2HexNAc_2$, and d_4-PA $dHex_1Hex_2HexNAc_2$, respectively (Fig. 3a). The intensity ratio of these ions suggested that the level of $dHex_1Hex_2HexNAc_2$ increased 3·6-fold in the SLE-model mouse. The structure of this oligosaccharide was estimated to be a core-fucosylated trimannosyl core lacking a Man residue from the successive cleavages of Man (Y_3: *m/z* 815), Man (Y_2: *m/z* 653), GlcNAc (Y_1: *m/z* 450) and Fuc ($Y_{1/1'}$: *m/z* 304) (inset in Fig. 3b). Such a defective *N*-glycan is known as a paucimannose-type glycan, and is rarely found in vertebrates. All paucimannose-type glycans, such as $dHex_1Hex_3HexNAc_2$ (a core-fucosylated trimannosyl core) and $Hex_3HexNAc_2$ (a non-fucosylated trimannosyl core) were increased in the SLE-model mouse. Furthermore, a two-fold increase was found in $Hex_4HexNAc_2$ (Man-4).

Figure 4 shows the molecular ratios of individual *N*-glycans between the SLE-model mice and control mice. A remarkable increase (3·5-fold) was also found in $dHex_1Hex_3HexNAc_4$, which is assigned to a core-fucosylated biantennary oligosaccharide lacking two non-reducing terminal Gal residues; its non-fucosylated form ($Hex_3HexNAc_4$) was also increased 1·8-fold in the SLE-model mouse. In other complex-type glycans, $dHex_1Hex_4HexNAc_4$ (1), which is assigned to a biantennary oligosaccharide lacking one molecule of Gal, increased 1·6-fold. Interestingly, a significant decrease was found in $dHex_1Hex_4HexNAc_4$ (2), a positional isomer of $dHex_1Hex_4HexNAc_4$ (1); this might have been caused by galactosylation on either GlcNAc-Manα1–3 or GlcNAc-Manα1–6. In contrast, no change was found between fucosylated and non-fucosylated oligosaccharides, nor between bisected and non-bisected oligosaccharides.

A significant increase was found in some high-mannose-type oligosaccharides, such as $Hex_5HexNAc_2$ (Man-5; + 137%) and $Hex_6HexNAc_2$ (1) (Man-6; + 136%), while $Hex_7HexNAc_2$ (1,2) (Man-7) and a positional isomer of $Hex_6HexNAc_2$ (1) [$Hex_6HexNAc_2$ (2)] remained unchanged in the SLE-model mouse. A slight increase was found in $Hex_8HexNAc_2$ (Man-8; + 116%) and $Hex_{10}HexNAc_2$ (possibly assigned to Man-9 plus Glc; + 116%).

Decreased oligosaccharides in the SLE-model mouse

The mass spectrum of the most decreased glycan is shown in Fig. 5(a). Based on differences of 0·5 U in *m/z* values among monoisotopic ions, molecular ions at *m/z* 1180·97

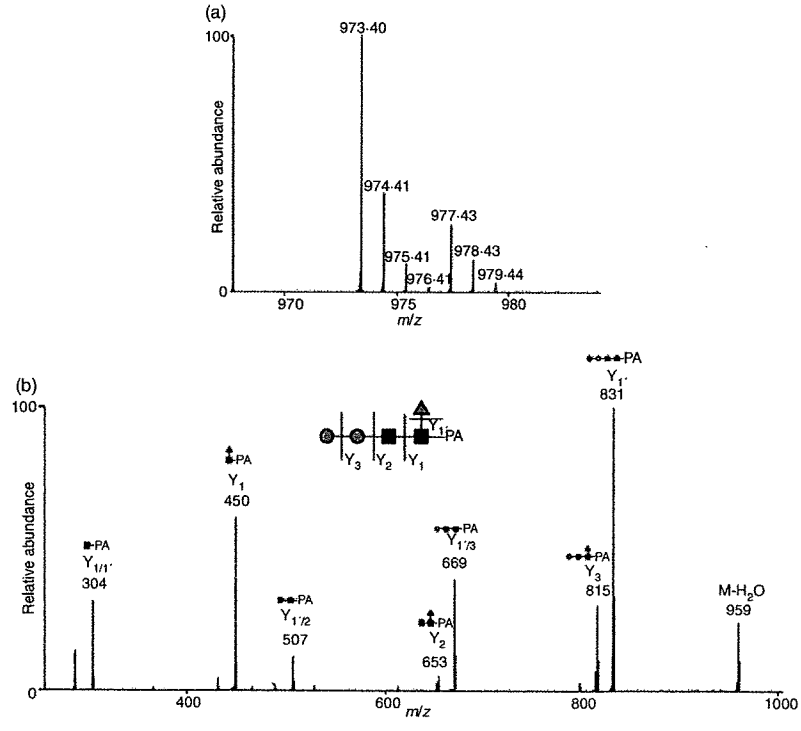

Figure 3. Mass (a) and mass spectrometry (MS)/MS (b) spectra of the most increased glycan ($dHex_1Hex_2HexNAc_2$). Precursor ion, *m/z* 973·4; grey circle, mannose; grey triangle, fucose; black square, *N*-acetylglucosamine.

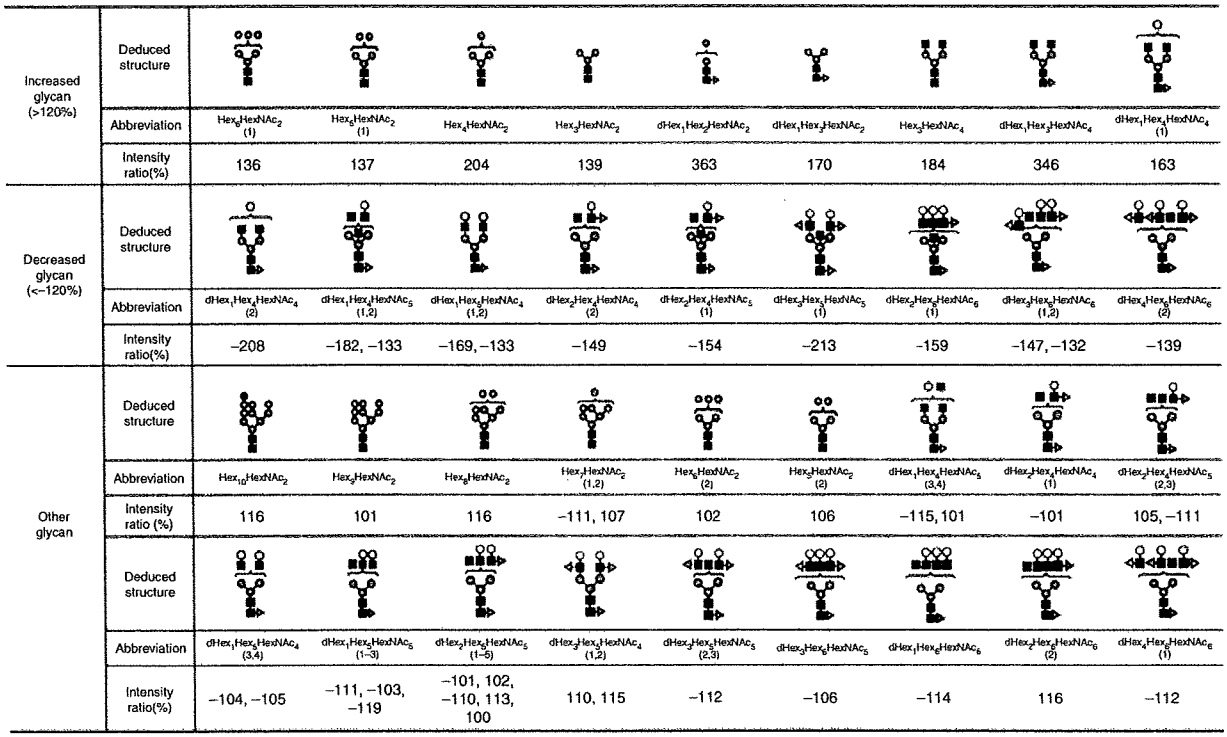

Figure 4. Summary of quantitative analysis of the systemic lupus erythematosus (SLE) model mouse against control mice. Values of relative ratios are the averages of three biological repeats. Grey circle, mannose; white circle, galactose; grey triangle, fucose; black square, *N*-acetylglucosamine.

and 1182·98 are estimated to be $[M + 2H]^{2+}$ of d_0-PA and d_4-PA $dHex_3Hex_5HexNAc_5$ (1), respectively. The intensity ratio of d_0 : d_4 glycans suggests that this glycan in the SLE-model mouse was decreased to 47% of the amount found in the control mouse. Figure 5(b) shows the MS^{2-4} spectra of d_0-PA $dHex_3Hex_5HexNAc_5$ (1) (precursor ion, *m/z* 1180·97). The fragment ion at *m/z* 512 in MS/MS (i) and MS/MS/MS (ii) spectra, which corresponds to $dHex_1Hex_1HexNAc_1^+$, suggests the attachment of two Lewis motifs on the side chains of the glycan. The presence of $dHex_1HexNAc_1PA^+$ (*m/z* 446) and $dHex_1Hex_1HexNAc_3PA^+$ (*m/z* 1015) reveals the linkages of a core fucose and a bisecting GlcNAc. Based on these fragments, this decreased glycan is estimated to be a Lewis-motif-modified, core-fucosylated and bisected biantennary oligosaccharide (inset in Fig. 5).

As shown in Figs 2(b) and 4, oligosaccharides lacking one molecule of Gal with and without bisecting GlcNAc [$dHex_1Hex_4HexNAc_4$ (2) and $dHex_1Hex_4HexNAc_5$ (1)] were decreased to 48% and 55%, respectively. A significant decrease was also found in other monogalactobiantennary oligosaccharides, such as $dHex_2Hex_4HexNAc_4$ (2) (a Lewis-motif-modified, core-fucosylated monogalacto-biantennary) and $dHex_2Hex_4HexNAc_5$ (1) (a Lewis-motif-modified core-fucosylated and bisected monogalacto-biantennary).

The oligosaccharides, non-reducing ends of which are fully galactosylated, were decreased in the SLE-model mouse. For example, monofucosyl biantennary $dHex_1Hex_5HexNAc_4$ (1) and (2) were decreased 59% and 75%, respectively. The di-, tri- and tetra-fucosylated oligosaccharides, $dHex_2Hex_6HexNAc_6$ (1), $dHex_3Hex_6HexNAc_6$ (1,2) and $dHex_4Hex_6HexNAc_6$ (1,2), which were estimated to be tri- and tetraantennary forms, were also significantly decreased. These results show that oligosaccharides with a complicated structure, such as high branching oligosaccharides and di- and tri-fucosylated oligosaccharides, were decreased in the SLE-model mouse.

Discussion

Using the isotope-tagging method, we demonstrated aberrant *N*-glycosylation on the kidney proteins of a SLE-model mouse. We found increases in low-molecular-mass glycans with simple structures, including paucimannose-type glycans, agalacto-biantennary oligosaccharides, Man-5 and Man-6, and decreases in glycans which have a complicated and diverse structure, such as digalacto-biantennary oligosaccharides and highly fucosylated glycans (Fig. 4). An increase in agalacto-biantennary oligosaccharides on IgG has been reported in the sera of patients with autoimmune diseases, including SLE, rheumatoid arthritis and IgA

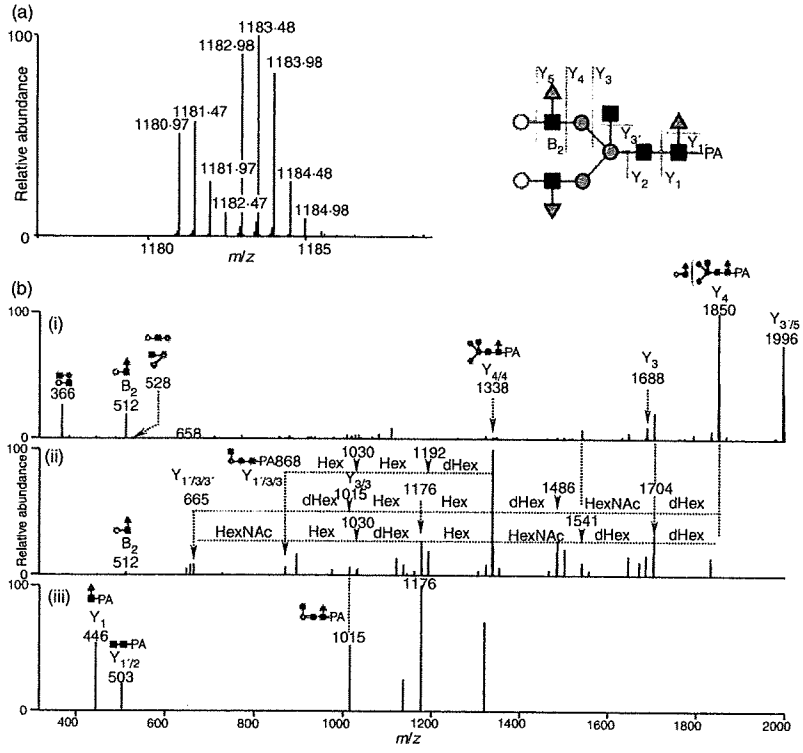

Figure 5. (a) Mass spectrum of the most decreased glycan [$dHex_3Hex_5HexNAc_5$ (1)]; (b-i) Mass spectrometry (MS)/MS spectrum of *m/z* 1181·0; (b-ii) MS/MS/MS spectrum of *m/z* 1849·7; (b-iii) MS/MS/MS/MS spectrum of *m/z* 1338·3. Grey circle, mannose; white circle, galactose; grey triangle, fucose; black square, *N*-acetylglucosamine; dHex, deoxyhexose (fucose); Hex, hexose (mannose and galactose); HN, *N*-acetylhexosamine (*N*-acetylglucosamine).

nephropathy.[9,11,28] The present findings show that abnormal glycosylation occurs not only in IgG in serum but also in several glycoproteins in the SLE-model mouse kidney.

Figure 6 shows the biosynthesis pathway of *N*-linked oligosaccharides in mammalian cells. Man-9, a product in the early stage of the pathway, is processed to Man-5 in the endoplasmic reticulum, and a GlcNAc and Fuc are added to Man-5 in the Golgi apparatus. After the removal of two Man residues by αM-II, GlcNAc, Gal and Fuc are further added to oligosaccharides by several glycosyltransferases. There have been a few reports on paucimannose-type oligosaccharides in vertebrates;[29] however, these glycans are common oligosaccharides in other multicellular organisms such as insects and *Caenorhabditis elegans*.[30,31] The membrane protease β-*N*-acetylglucosaminidase is thought to mediate the synthesis of paucimannose-type oligosaccharides.[32] Based on core fucosylation on some paucimannose-type oligosaccharides, it was deduced that β-*N*-acetylglucosaminidase might act on glycan synthesis after *N*-acetylglucosaminyltransferase I, core fucosyltransferase and αM-II.[32] The synthesis of paucimannose-type oligosaccharides may be involved in the suppression of growing diversity and complexity of glycan structures.

We found a number of changes in the levels of monogalacto-biantennary oligosaccharides in the SLE mouse. Galactosylation to agalacto-biantennary oligosaccharides is mediated by β-1,4-galactosyltransferase

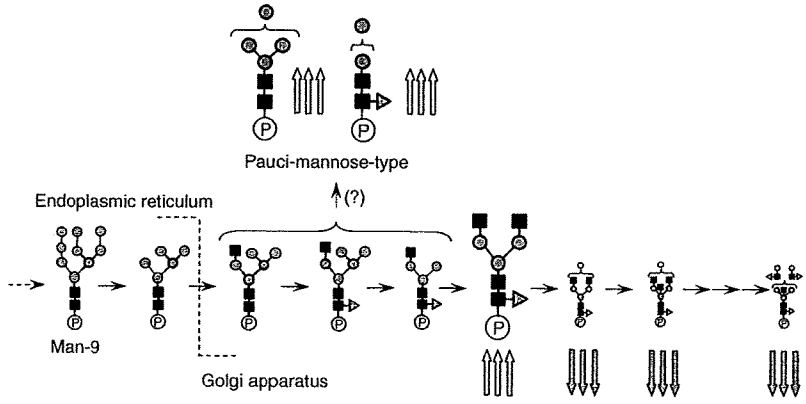

Figure 6. Biosynthesis pathway of *N*-linked oligosaccharides in mammalian cells. Triple up-arrow, increases of more than +2·0; triple down-arrow, decreases of not more than −2·0. Grey circle, mannose; white circle, galactose; grey triangle, fucose; black square, *N*-acetylglucosamine. 'P' is protein portion.

(β-1,4-GalTase).[33] Previous studies suggested that translational repression of β-1,4-GalTase in lymphocytes is associated with an increase in agalacto-oligosaccharides on IgG in the serum of the MRL-lpr mouse.[34] Although the activity of β-1,4-GalTase remains unknown in the SLE-model mouse, the increase in agalacto forms and the decrease in digalacto forms imply changes in β-1,4-GalTase activity. The present results suggest a decrease in diverse and complex glycans, which are synthesized at a late stage in the *N*-glycan synthesis pathway, and an increase in the simple glycans appearing at an early stage in the SLE-model mouse.

The activation of complements is involved in glomerular nephritis of SLE.[35–37] The complements are activated through three pathways: a classical pathway, an alternative pathway and a lectin pathway. In the classical pathway, a binding of C1q to an immune complex triggers the activation of C1r and C1s. Activated C1s cleaves C4 and C2, generating C3 convertase (C4b2a), which generates C3b. The complement component subsequently produces C5b-9 complex, which leads to an inflammatory response on host tissues.[38–41] The excess deposition of immune complexes followed by a sustained immune response triggers tissue disorders, including lupus nephritis.[42–45] In the lectin pathway, mannose-binding lectin (MBL) is associated with the activation of complements. Two forms of MBL (MBL-A and MBL-C) are present in complexes with MBL-associated serine proteases (MASPs) in mice. The MASPs are activated by binding MBL to Man or GlcNAc on the surface of the antigen in a calcium-dependent manner.[46–49] Like C1s in the classical pathway, activated MASPs cleave C4 and C2.[50,51] In lupus nephritis, MBL-A and MBL-C in the immune complex bind to GlcNAc residues at the reducing ends of agalacto-biantennary oligosaccharides in IgG,[52] and subsequently activate the complements.[53,54] In αM-II-deficient mice, which suffer from SLE-like syndromes including kidney disorders, the majority of glycans are hybrid-type oligosaccharides because of the failure of Man trimming by the lack of αM-II.[16] Green *et al.* concluded that MBL recognized Manα1–3 and Manα1–6 linkages in hybrid-type oligosaccharides,[17] and glycans lacking normal side chains, including agalacto-biantennary oligosaccharides, might be involved in the aberrant immune response in autoimmune diseases. Paucimannose glycans, which contain exposed Manα1–3 or Manα1–6 linkages, may be recognized as ligand carbohydrates by MBL. Our present finding, an increase in paucimannose oligosaccharides and agalacto forms, might result from an alteration of the biosynthesis pathway of *N*-glycans. The alterations may cause the aberrant glycosylations on most of the glycoproteins rather than some glycoproteins in the SLE-model mouse. The changes in glycosylation might be involved in an autoimmune pathogenesis in the SLE-model mouse kidney.

The continuous production of aberrant antibodies that react with components from self-tissue and accumulation in the immune complex are thought to promote tissue damage in autoimmune disease.[55,56] The mechanism of localized accumulation in the immune complex in some tissues remains unknown in SLE. We found an increase in glycans that may bind to MBL and subsequently promote complement activation via the lectin pathway in the mouse kidney. Our present results suggest that an aberrant *N*-glycan synthesis pathway as well as an abnormal immune system may be involved in the damage caused by glomerular nephritis in the SLE-model mouse.

Acknowledgements

This study was supported in part by a Grant-in-Aid from the Ministry of Health, Labor, and Welfare, and Core Research for the Evolutional Science and Technology Program (CREST), Japan Science and Technology Corp (JST).

References

1 Dwek RA. Glycobiology: toward understanding the function of sugars. *Chem Rev* 1996; **96**:683–720.
2 Helenius A, Aebi M. Intracellular functions of N-linked glycans. *Science* 2001; **291**:2364–9.
3 Zak I, Lewandowska E, Gnyp W. Selectin glycoprotein ligands. *Acta Biochim Pol* 2000; **47**:393–412.
4 Axford JS. Glycosylation and rheumatic disease. *Biochim Biophys Acta* 1999; **1455**:219–29.
5 Feizi T, Gooi HC, Childs RA, Picard JK, Uemura K, Loomes LM, Thorpe SJ, Hounsell EF. Tumour-associated and differentiation antigens on the carbohydrate moieties of mucin-type glycoproteins. *Biochem Soc Trans* 1984; **12**:591–6.
6 Kannagi R, Izawa M, Koike T, Miyazaki K, Kimura N. Carbohydrate-mediated cell adhesion in cancer metastasis and angiogenesis. *Cancer Sci* 2004; **95**:377–84.
7 Goodarzi MT, Turner GA. Decreased branching, increased fucosylation and changed sialylation of alpha-1-proteinase inhibitor in breast and ovarian cancer. *Clin Chim Acta* 1995; **236**:161–71.
8 Yamashita K, Fukushima K, Sakiyama T, Murata F, Kuroki M, Matsuoka Y. Expression of Sia alpha 2→6Gal beta 1→4GlcNAc residues on sugar chains of glycoproteins including carcinoembryonic antigens in human colon adenocarcinoma: applications of *Trichosanthes japonica* agglutinin I for early diagnosis. *Cancer Res* 1995; **55**:1675–9.
9 Tomana M, Schrohenloher RE, Reveille JD, Arnett FC, Koopman WJ. Abnormal galactosylation of serum IgG in patients with systemic lupus erythematosus and members of families with high frequency of autoimmune diseases. *Rheumatol Int* 1992; **12**:191–4.
10 Mizuochi T, Hamako J, Nose M, Titani K. Structural changes in the oligosaccharide chains of IgG in autoimmune MRL/Mp-lpr/lpr mice. *J Immunol* 1990; **145**:1794–8.
11 Arnold JN, Wormald MR, Sim RB, Rudd PM, Dwek RA. The impact of glycosylation on the biological function and structure

of human immunoglobulins. *Annu Rev Immunol* 2007; **25**:21–50.

12 Das H, Atsumi T, Fukushima Y *et al.* Diagnostic value of anti-agalactosyl IgG antibodies in rheumatoid arthritis. *Clin Rheumatol* 2004; **23**:218–22.

13 Raghav SK, Gupta B, Agrawal C, Saroha A, Das RH, Chaturvedi VP, Das HR. Altered expression and glycosylation of plasma proteins in rheumatoid arthritis. *Glycoconj J* 2006; **23**:167–73.

14 Elliott MA, Elliott HG, Gallagher K, McGuire J, Field M, Smith KD. Investigation into the concanavalin A reactivity, fucosylation and oligosaccharide microheterogeneity of alpha 1-acid glycoprotein expressed in the sera of patients with rheumatoid arthritis. *J Chromatogr B Biomed Sci Appl* 1997; **688**:229–37.

15 Rops AL, van den Hoven MJ, Bakker MA *et al.* Expression of glomerular heparan sulphate domains in murine and human lupus nephritis. *Nephrol Dial Transplant* 2007; **22**:1891–902.

16 Chui D, Sellakumar G, Green R *et al.* Genetic remodeling of protein glycosylation *in vivo* induces autoimmune disease. *Proc Natl Acad Sci USA* 2001; **98**:1142–7.

17 Green RS, Stone EL, Tenno M, Lehtonen E, Farquhar MG, Marth JD. Mammalian *N*-glycan branching protects against innate immune self-recognition and inflammation in autoimmune disease pathogenesis. *Immunity* 2007; **27**:308–20.

18 Wada Y. Mass spectrometry in the detection and diagnosis of congenital disorders of glycosylation. *Eur J Mass Spectrom (Chichester, Eng)* 2007; **13**:101–3.

19 Faid V, Chirat F, Seta N, Foulquier F, Morelle W. A rapid mass spectrometric strategy for the characterization of *N*- and *O*-glycan chains in the diagnosis of defects in glycan biosynthesis. *Proteomics* 2007; **7**:1800–13.

20 Miyamoto S. Clinical applications of glycomic approaches for the detection of cancer and other diseases. *Curr Opin Mol Ther* 2006; **8**:507–13.

21 Yuan J, Hashii N, Kawasaki N, Itoh S, Kawanishi T, Hayakawa T. Isotope tag method for quantitative analysis of carbohydrates by liquid chromatography-mass spectrometry. *J Chromatogr A* 2005; **1067**:145–52.

22 Alvarez-Manilla G, Warren NL, Abney T, Atwood J III, Azadi P, York WS, Pierce M, Orlando R. Tools for glycomics: relative quantitation of glycans by isotopic permethylation using 13CH3I. *Glycobiology* 2007; **17**:677–87.

23 Kang P, Mechref Y, Kyselova Z, Goetz JA, Novotny MV. Comparative glycomic mapping through quantitative permethylation and stable-isotope labeling. *Anal Chem* 2007; **79**:6064–73.

24 Bowman MJ, Zaia J. Tags for the stable isotopic labeling of carbohydrates and quantitative analysis by mass spectrometry. *Anal Chem* 2007; **79**:5777–84.

25 Watanabe-Fukunaga R, Brannan CI, Copeland NG, Jenkins NA, Nagata S. Lymphoproliferation disorder in mice explained by defects in Fas antigen that mediates apoptosis. *Nature* 1992; **356**:314–7.

26 Adachi M, Watanabe-Fukunaga R, Nagata S. Aberrant transcription caused by the insertion of an early transposable element in an intron of the Fas antigen gene of lpr mice. *Proc Natl Acad Sci USA* 1993; **90**:1756–60.

27 Merino R, Iwamoto M, Fossati L, Izui S. Polyclonal B cell activation arises from different mechanisms in lupus-prone (NZB × NZW)F_1 and MRL/MpJ-lpr/lpr mice. *J Immunol* 1993; **151**:6509–16.

28 Homma H, Tozawa K, Yasui T, Itoh Y, Hayashi Y, Kohri K. Abnormal glycosylation of serum IgG in patients with IgA nephropathy. *Clin Exp Nephrol* 2006; **10**:180–5.

29 Hase S, Okawa K, Ikenaka T. Identification of the trimannosylchitobiose structure in sugar moieties of Japanese quail ovomucoid. *J Biochem* 1982; **91**:735–7.

30 Kubelka V, Altmann F, Kornfeld G, Marz L. Structures of the N-linked oligosaccharides of the membrane glycoproteins from three lepidopteran cell lines (Sf-21, IZD-Mb-0503, Bm-N). *Arch Biochem Biophys* 1994; **308**:148–57.

31 Natsuka S, Adachi J, Kawaguchi M, Nakakita S, Hase S, Ichikawa A, Ikura K. Structural analysis of N-linked glycans in *Caenorhabditis elegans*. *J Biochem* 2002; **131**:807–13.

32 Altmann F, Schwihla H, Staudacher E, Glossl J, Marz L. Insect cells contain an unusual, membrane-bound beta-*N*-acetylglucosaminidase probably involved in the processing of protein *N*-glycans. *J Biol Chem* 1995; **270**:17344–9.

33 Guo S, Sato T, Shirane K, Furukawa K. Galactosylation of N-linked oligosaccharides by human beta-1,4-galactosyltransferases I, II, III, IV, V, and VI expressed in Sf-9 cells. *Glycobiology* 2001; **11**:813–20.

34 Jeddi PA, Lund T, Bodman KB *et al.* Reduced galactosyltransferase mRNA levels are associated with the agalactosyl IgG found in arthritis-prone MRL-lpr/lpr strain mice. *Immunology* 1994; **83**:484–8.

35 Cameron JS. Lupus nephritis. *J Am Soc Nephrol* 1999; **10**:413–24.

36 Walport MJ. Complement. First of two parts. *N Engl J Med* 2001; **344**:1058–66.

37 Walport MJ. Complement. Second of two parts. *N Engl J Med* 2001; **344**:1140–4.

38 Botto M. Links between complement deficiency and apoptosis. *Arthritis Res* 2001; **3**:207–10.

39 Hanayama R, Tanaka M, Miyasaka K, Aozasa K, Koike M, Uchiyama Y, Nagata S. Autoimmune disease and impaired uptake of apoptotic cells in MFG-E8-deficient mice. *Science* 2004; **304**:1147–50.

40 Arason GJ, Steinsson K, Kolka R, Vikingsdottir T, D'Ambrogio MS, Valdimarsson H. Patients with systemic lupus erythematosus are deficient in complement-dependent prevention of immune precipitation. *Rheumatology (Oxford)* 2004; **43**:783–9.

41 Cook HT, Botto M. Mechanisms of disease: the complement system and the pathogenesis of systemic lupus erythematosus. *Nat Clin Pract Rheumatol* 2006; **2**:330–7.

42 Gunnarsson I, Sundelin B, Heimburger M, Forslid J, van Vollenhoven R, Lundberg I, Jacobson SH. Repeated renal biopsy in proliferative lupus nephritis – predictive role of serum C1q and albuminuria. *J Rheumatol* 2002; **29**:693–9.

43 Buyon JP, Tamerius J, Belmont HM, Abramson SB. Assessment of disease activity and impending flare in patients with systemic lupus erythematosus. Comparison of the use of complement split products and conventional measurements of complement. *Arthritis Rheum* 1992; **35**:1028–37.

44 Markiewski MM, Lambris JD. The role of complement in inflammatory diseases from behind the scenes into the spotlight. *Am J Pathol* 2007; **171**:715–27.

45 Sturfelt G. The complement system in systemic lupus erythematosus. *Scand J Rheumatol* 2002; **31**:129–32.

46 Holmskov U, Malhotra R, Sim RB, Jensenius JC. Collectins: collagenous C-type lectins of the innate immune defense system. *Immunol Today* 1994; **15**:67–74.

47 Weis WI, Drickamer K, Hendrickson WA. Structure of a C-type mannose-binding protein complexed with an oligosaccharide. *Nature* 1992; **360**:127–34.
48 Takahashi M, Mori S, Shigeta S, Fujita T. Role of MBL-associated serine protease (MASP) on activation of the lectin complement pathway. *Adv Exp Med Biol* 2007; **598**:93–104.
49 Turner MW. Mannose-binding lectin: the pluripotent molecule of the innate immune system. *Immunol Today* 1996; **17**:532–40.
50 Holmskov U, Malhotra R, Sim RB, Jensenius JC. Collectins: collagenous C-type lectins of the innate immune defense system. *Immunol Today* 1994; **15**:67–74.
51 Thiel S, Vorup-Jensen T, Stover CM *et al.* A second serine protease associated with mannan-binding lectin that activates complement. *Nature* 1997; **386**:506–10.
52 Lhotta K, Wurzner R, Konig P. Glomerular deposition of mannose-binding lectin in human glomerulonephritis. *Nephrol Dial Transplant* 1999; **14**:881–6.
53 Ohsawa I, Ohi H, Tamano M *et al.* Cryoprecipitate of patients with cryoglobulinemic glomerulonephritis contains molecules of the lectin complement pathway. *Clin Immunol* 2001; **101**:59–66.
54 Trouw LA, Seelen MA, Duijs JM *et al.* Activation of the lectin pathway in murine lupus nephritis. *Mol Immunol* 2005; **42**:731–40.
55 Jorgensen TN, Gubbels MR, Kotzin BL. New insights into disease pathogenesis from mouse lupus genetics. *Curr Opin Immunol* 2004; **16**:787–93.
56 Lauwerys BR, Wakeland EK. Genetics of lupus nephritis. *Lupus* 2005; **14**:2–12.

Available online at www.sciencedirect.com
ScienceDirect
Biologicals 36 (2008) 27–36
BIOLOGICALS
www.elsevier.com/locate/biologicals

Prion removal by nanofiltration under different experimental conditions

Mikihiro Yunoki [a,b,*], Hiroyuki Tanaka [b], Takeru Urayama [a,b], Shinji Hattori [b], Masahiro Ohtani [b], Yuji Ohkubo [b], Yoshiyasu Kawabata [b], Yuuki Miyatake [b], Ayako Nanjo [b], Eiji Iwao [c], Masanori Morita [b], Elaine Wilson [d], Christine MacLean [d], Kazuyoshi Ikuta [a]

[a] *Department of Virology, Research Institute for Microbial Diseases, Osaka University, Japan*
[b] *Research & Development Division, Benesis Corporation, Japan*
[c] *Pharmaceutical Research Division, Mitsubishi Pharma Corporation, Japan*
[d] *BioReliance, Invitrogen BioServices, UK*

Received 21 December 2006; revised 11 April 2007; accepted 27 April 2007

Abstract

Manufacturing processes used in the production of biopharmaceutical or biological products should be evaluated for their ability to remove potential contaminants, including TSE agents. In the present study, we have evaluated scrapie prion protein (PrP^{Sc}) removal in the presence of different starting materials, using virus removal filters of different pore sizes. Following 75 nm filtration, PrP^{Sc} was detected in the filtrate by Western blot (WB) analysis when a "super-sonicated" microsomal fraction derived from hamster adapted scrapie strain 263K (263K MF) was used as the spike material. In contrast, no PrP^{Sc} was detected when an untreated 263K MF was used. By using spike materials prepared in a manner designed to optimize the particle size distribution within the preparation, only 15 nm filtration was shown to remove PrP^{Sc} to below the limits of detection of the WB assays used under all the experimental conditions. However, infectious PrP^{Sc} was recovered following 15 nm filtration under one experimental condition. The results obtained suggest that the nature of the spike preparation is an important factor in evaluating the ability of filters to remove prions, and that procedures designed to minimize the particle size distribution of the prion spike, such as the "super-sonication" or detergent treatments described herein, should be used for the preparation of the spike materials.

Keywords: Prion; Removal; Filter; Clearance study; Spike material

1. Introduction

The transmission of variant Creutzfeldt–Jakob disease (vCJD) through blood transfusion has been of increasing concern, since a fourth possible transmission case was reported [1]. In addition, prions have been detected in the buffy coat separated from the blood of hamsters infected with scrapie, using a biochemical assay (protein misfolding cyclic amplification, or PMCA) [2]. Infectious prions are thought to be the causative agent of the transmissible spongiform encephalopathy (TSE) diseases, which include Creutzfeldt–Jakob disease (CJD), vCJD, and bovine spongiform encephalopathy (BSE). Therefore, to reduce the risk of transmission when raw materials for protein products (such as plasma) are contaminated with infectious prions, measures should be introduced to decrease the prion load, to evaluate the risk to the product, and to introduce prion removal/inactivation step(s) in the manufacturing process, if feasible [3–5]. Unlike viruses, the minimum infectious prion unit does not exist as a single particle. The infectious prion unit is believed to be composed of protein polymers/aggregates, rather than a prion particle. The unusual nature of the prion agent makes it particularly important to

* Corresponding author. Hirakata Research Laboratory, Research & Development Division, Benesis Corporation, 2-25-1 Shodai-Ohtani, Hirakata, Osaka 573-1153, Japan. Tel.: +81 72 850 0100; fax: +81 72 864 2341.
E-mail address: yunoki.mikihiro@mk.m-pharma.co.jp (M. Yunoki).

1045-1056/07/$34.00
doi:10.1016/j.biologicals.2007.04.005

consider the effect of the prion spike material when evaluating process steps for prion clearance. A rationale for the choice of the spike preparation used for such evaluation studies should be provided [4].

Several prion strains have been used to evaluate manufacturing processes for their ability to remove TSE agents, including hamster scrapie prion protein (PrP^{Sc}, 263K or Sc237), and mouse PrP^{BSE} (301V). In a polyethylene glycol (PEG) fractionation process, hamster PrP^{Sc} and human PrP^{vCJD}, prepared using the same methodology, were reported to behave in a very similar manner [6]. Different prion spike preparations have been used to investigate prion removal, including crude brain homogenate (BH), microsomal fraction (MF), caveolae-like domains (CLDs), and purified PrP^{Sc}. Of these materials, purified PrP^{Sc} was reported to behave differently from the other preparations in an 8% ethanol fractionation step [7]. This result suggests that the methods used to prepare the prion spike material may be a critical factor in prion clearance studies. Furthermore, these reports are useful in providing a rationale for the choice of the prion source and spike preparation used for such evaluation studies [8].

Tateishi et al. reported that sarkosyl influenced the ability of BMM40 filters to remove prions, using BH derived from CJD-infected mice [9]. The presence of sarkosyl was also shown to significantly reduce the capacity of Planova (P)-35N to remove the scrapie agent ME7, while filtration with P-15N resulted in the complete removal of infectivity, to below the limit of detection of the bioassay used, in both the presence and absence of sarkosyl [10]. Van Holten et al. evaluated the capacity of Viresolve 180 membranes (designed for virus removal from proteins of <180 kDa) to remove prions by using BH which was lysolecithin-treated, sonicated, and subsequently passed through a 100 nm filter (SBH), and demonstrated removal of PrP^{Sc} down to the limit of detection of the Western blot assay used. They argued that by using a better defined spike material, where the size of the scrapie particles was limited, the results may be more relevant with respect to the removal of potential TSE infectivity in plasma than previous studies that used a less well-defined BH [11].

Aggregation of the prion protein is a critical parameter when evaluating nanofiltration steps. The actual form of the infectious agent present in plasma in natural infection is not known. In addition, nanofiltration is typically performed late in the downstream processing, after protein purification steps, which may result in removal of larger or aggregated prion forms. Therefore, use of a spike preparation containing large aggregates may result in an over-estimate of the prion removal capacity of a filter. Although the reports described above, and others, have shown excellent prion removal ability for a number of filters, most reports have not described the particle size distribution of the prion protein in the spike preparations used. Therefore, in this study we have investigated the prion removal capacity of P-35N, P-20N and P-15N filters under diverse conditions, considering the particle size distribution of the MF preparations used.

2. Materials and methods

2.1. Preparation of microsomal fraction (MF)

Brains removed from hamsters infected with scrapie strain 263K [12] (originally obtained from the Institute for Animal Health, Edinburgh, UK), were homogenized in phosphate buffered saline (PBS) until homogeneous, to a final concentration of 10% (w/v). The homogenate was clarified by low speed centrifugation, to remove larger cell debris and nuclei, and the supernatant material was then further clarified by centrifugation at 8,000 × *g* for 10 min at 4 °C, before being ultracentrifuged at 141,000 × *g* for 60 min at 4 °C, to concentrate the scrapie fibrils, and small membrane vesicles and fragments. The pelleted material was resuspended in PBS, aliquoted, and stored at −80 °C. This material was designated 263K MF. Prior to use, stocks were thawed at 37 °C, and sonicated 2 × 4 min on ice water (Ultrawave ultrasonic bath model #U100, 130 W 30 kHz, Ultrawave Ltd., Cardiff, UK). Six independent batches of 263K MF were used in this study. These batches are designated 263K MF preparation lots A–F (Tables 1–3). Normal MF, derived from normal (i.e. uninfected) hamster brain material, was also prepared as described above.

Since we were unable to measure the particle size distribution of contaminated materials in our facility, we used normal MF, and investigated changes in the particle size distribution following strong sonication or treatment with detergent. Various concentrations of sarkosyl (*N*-lauroylsarcosine sodium salt, Nacalai Tesque, Inc., Kyoto, Japan), lysolecithin (L-α-lysophosphatidylcholine, Sigma-Aldrich Corp., St. Louis, USA), Triton X-100 (polyethylene glycol mono-*p*-isooctylphenyl ether, Nacalai Tesque, Inc.), TNBP (tri-n-butyl phosphate, Wako Pure Chemical Industries, Ltd., Osaka, Japan), and/or 1% Tween 80 (Nacalai Tesque, Inc.) were added to normal MF. Changes in the particle size distribution were then monitored by dynamic light scattering method using volume-weighted gaussian analysis using a submicrometer particle sizer (NICOMP Type 370, Particle Sizing Systems, Inc., Santa Barbara, USA). To evaluate the effect of strong sonication, normal MF was sonicated using a closed system ultrasonic cell disruptor (Bioruptor UCD-200T, CosmoBio Co. Ltd., Tokyo, Japan) with a resonance chip set in the tube. Sonication was performed for 1 min at 20 kHz, 200 W in a cold water-bath. Ten cycles of sonication were performed, with a 1 min

Table 1
Scrapie infectivity in different 263K MF preparations[a]

	Log_{10} LD_{50}/ml	SE at 95% probability
Non-super-sonicated 263K MF lot C	5.7	0.44
Super-sonicated 263K MF lot C	6.0	0.53
Super-sonicated 263K MF lot D	5.3	0.69
SD-treated, ultracentrifuged, super-sonicated and 220 nm-filtered 263K MF lot C	6.9	0.69

[a] This bioassay study was performed in accordance with GLP regulations.

Table 2
Removal of PrP^{Sc} from PrP^{Sc}-inoculated PBS

	PVDF filter				Planova filter					
	220 nm		100 nm		P-75N (72 ± 2 nm)		P-35N (35 ± 2 nm)		P-15N (15 ± 2 nm)	
Super-sonicated	+	−	+	−	+	−	+	−	+	−
Before filtration	4.2/3.5[a]	3.5/4.2	4.2/3.5	3.5/4.2	4.2/4.2	3.5/4.2	4.2/4.2	3.5/4.2	4.2/4.2	3.5/4.2
Filtered	3.8/3.8	3.1/3.8	3.8/3.1	2.4/3.1	2.4/2.4	<1.0/<1.0	<1.0/<1.0	<1.0/<1.0	<1.0/<1.0	<1.0/<1.0
LRF[b]	0.4/−0.3	0.4/0.4	0.4/0.4	1.1/1.1	1.8/1.8	≥2.5/≥3.2	≥3.2/≥3.2	≥2.5/≥3.2	≥3.2/≥3.2	≥2.5/≥3.2

Data represents total PrP^{Sc} present in samples, expressed as $\log_{10}$ arbitrary units, following Western blot analysis as described for WB1. This study was performed in accordance with GLP regulations.

[a] Two independent batches of 263K MF were used: lot C (left) and lot D (right), respectively.

[b] LRF, log reduction factor = total PrP^{Sc} in input/total PrP^{Sc} in filtrate, expressed as a $\log_{10}$ value.

interval between each sonication treatment. During the treatment cycle, the particle size distribution was monitored. We named this treatment cycle "super-sonication".

Different preparations of 263K MF, treated with various combinations of detergent, ultracentrifugation and/or "super-sonication", were used as the spiking agent in the process evaluation studies, and are described in the relevant methods sections below.

2.2. Detection of PrP^{Sc} by Western blotting (WB)

To determine the relative levels of PrP^{Sc} present in different samples, WB assays were performed. Three slightly different WB methodologies were applied over the course of the studies, all of which are based on detection of the disease-associated, protease-resistant form of the prion protein (PrP^{Sc}), using the monoclonal antibody 3F4 (Signet Laboratories, Inc., Dedham, USA) [13]. WB methods 1 and 2 were developed independently, and use different approaches to calculate the titer of PrP^{Sc}. As these assays were performed as part of GLP studies intended for regulatory submission, the results are presented as reported in these studies.

2.2.1. Method 1 (WB1)

Samples and controls were either tested directly, or first ultracentrifuged at 141,000 × *g* for 60 min at 4 °C, and the pelleted material then resuspended in PBS. Ultracentrifugation was performed to concentrate the PrP^{Sc} present in large volume samples, and to remove soluble proteins or buffer components that might interfere with the WB assay. Samples were digested with proteinase K (Roche Diagnostics, GmbH, Penzberg, Germany) for 60 min at 37 °C. The optimal concentration of proteinase K, to remove any background that could interfere with the detection of PrP^{Sc} and to allow effective recovery of the PrP^{Sc} protein, was previously established for each sample. Digested samples were mixed 1:1 with Laemmli sample buffer (62.5 mM Tris–HCl, pH 6.8, 25% (v/v) glycerol, 2% (w/v) SDS, and 0.01% (w/v) bromophenol blue, BioRad Laboratories Inc., Hercules, USA) containing 5% (v/v) β-mercaptoethanol. After boiling, serial 5-fold dilutions of

Table 3
Removal of PrP^{Sc} from PrP^{Sc}-inoculated plasma preparations[a]

Filter	P-35N (35 ± 2 nm)		P-20N (19 ± 2 nm)		P-15N (15 ± 2 nm)			
Preparation	IVIG	Haptoglobin	IVIG	Haptoglobin	Antithrombin			Thrombin
Spike material	263K sMF[c]	263K sMF[c]	263K sMF[d]	263K dsMF[e]	263K dMF[f]	263K sMF[c]		263K dsMF[e]
MF preparation lot.	C/D	B	E/F	E/F	A/A	B		C/D
Spike ratio	1/100	1/200	1/20	1/200	1/50	1/21		1/20
Detection method[b]	WB1	WB3	WB2	WB2	WB1	WB3	BA	WB1
Before filtration	3.2/2.5	2.4	6.8/6.8	6.7/6.1	3.1/3.1	3.6	+ve	3.7/3.7
Filtered	0.8/0.8	<1.0	4.8/4.3	4.8/4.7	0.0/0.0	<0.8	+ve	<0.2/<0.2
Log reduction factor	2.4/1.7	≥1.4	2.0/2.5	1.9/1.4	≥3.1/≥3.1	≥2.8	NA	≥3.5/≥3.5

Abbreviations used: 263K MF, microsomal fraction derived from hamster adapted scrapie strain 263K; IVIG, intravenous immunoglobulin; 263K sMF, "super-sonicated" 263K MF; WB, Western blotting; 263K dsMF, detergent treated and "super-sonicated" 263K MF; 263K dMF, detergent treated 263K MF; BA, bioassay; +ve, scrapie positive.

[a] Scaled down conditions were designed according to current guidelines. However, in a study using P-35N filter and haptoglobin, clogging of the filter occurred, and the filtration was subsequently terminated.

[b] WB1, WB2, and WB3 mean Western blotting methods 1, 2 and 3, respectively. The studies involving the use of WB1 and WB2 were performed in accordance with GLP regulations; the studies involving the use of WB3 and the qualitative BA shown in this table, were performed as non-GLP studies.

[c] 263K MF was "super-sonicated" then 220 nm-filtered prior to spiking.

[d] 263K MF was ultracentrifuged at 141,000 × *g* for 60 min at 4 °C, resuspended in buffer equivalent to the starting material without protein, "super-sonicated", and 220 nm-filtered prior to spiking.

[e] 263K MF was "SD-treated", ultracentrifuged at 141,000 × *g* for 60 min at 4 °C, resuspended in the starting material (thrombin) or saline (haptoglobin), and "super-sonicated". These materials were 220 nm-filtered prior to spiking.

[f] 263K MF was treated with 0.1% sarkosyl for 30 min at room temperature.

the sample were then prepared and subjected to electrophoresis using 12% (w/v) SDS-polyacrylamide gels. Proteins were transferred from the gels to 0.45 μm PVDF membranes (Immobilon-P, Millipore Corp., Billerica, USA), and non-specific binding sites on the membranes were then blocked by overnight incubation in buffer containing dried milk and Tween 20. The blocked membranes were incubated with monoclonal antibody 3F4, washed extensively, and then incubated with a secondary horseradish peroxidase (HRP)-conjugated anti-mouse antibody (Sigma-Aldrich Corp.). After further extensive washing, bound antibody was detected using an ECL-Plus detection system (GE Healthcare UK Ltd, Buckinghamshire, UK) and exposure to blue-light sensitive film.

The level of PrP^{Sc} present in each sample was calculated based on the end-point dilution after analysis by WB. The end-point dilution for each titration was taken as the first dilution at which the 28 kDa PrP^{Sc} protein could not be detected. The reciprocal of this dilution was then taken as the titer of the agent, and expressed in arbitrary units/ml.

2.2.2. Method 2 (WB2)

WB was performed essentially as described by Lee et al. [14]. Briefly, samples were digested with proteinase K at approximately 6 U/ml for 60 min at 37 °C and centrifuged at approximately 20,000 × *g* for 60 min at 4 °C. The pellet was then resuspended and denatured in a 1:1 mix of supernatant and sample buffer (62.5 mM Tris–HCl, pH 6.8, 10% (v/v) glycerol, 2% (w/v) SDS and 0.0025% (w/v) bromophenol blue, Invitrogen Corp. Carlsbad, USA), by heating at approximately 100 °C. Serial 3.2-fold (0.5 $\log_{10}$) dilutions of the sample were prepared, and loaded onto 12% (w/v) SDS-polyacrylamide gels. Following electrophoresis, proteins were transferred to nitrocellulose membranes (Invitrogen Corp.), and the membranes blocked using buffer containing dried milk and Tween 20 for 1–2 h at room temperature. The blocked membranes were then incubated with monoclonal antibody 3F4, washed extensively, and incubated with a secondary alkaline phosphatase (AP)-conjugated anti-mouse antibody (Cambridge Biosciences Ltd., Cambridge, UK). After further extensive washing, bound antibody was detected using a CDP Star/Nitroblock II detection system (Applied Biosciences, Bedford, USA) and exposure to blue-light sensitive film.

The titer of PrP^{Sc} present in each sample was calculated slightly differently from WB1 and WB3. The end-point dilution for each titration was taken as the last dilution at which the 28 kDa PrP^{Sc} protein could be detected. The reciprocal of this dilution was then taken as the amount of agent in the sample volume tested, and was adjusted for the volume tested and any concentration factors, to give a titer/ml for the original process sample.

2.2.3. Method 3 (WB3)

Samples were ultracentrifuged twice at 150,000 × *g* for 1 h. The samples in the precipitates were then resuspended in PBS at 1/1 or 1/10th volume of the original. Resuspended samples were treated with proteinase K at a final concentration of 10–100 μg/ml. After incubation at 37 °C for 60 min, samples were treated with 10 mM 4-(2-aminoethyl)-benzene sulfonyl fluoride hydrochloride (AEBSF) at room temperature for 10 min, then mixed with 5× SDS-polyacrylamide gel electrophoresis (PAGE) sample buffer (300 mM Tris–HCl, 12% (w/v) SDS, 25% (v/v) glycerol, and 0.025% (w/v) bromophenol blue, pH 6.8, with 25% (v/v) β-mercaptoethanol) and heated at 100 °C for 5 min. Samples were serially 5-fold diluted with 1× PAGE dilution buffer (60 mM Tris–HCl, 2.4% (w/v) SDS, 5% (v/v) glycerol, and 0.005% (w/v) bromophenol blue, pH 6.8). SDS-PAGE was performed at 30 mA per gel for approximately 42 min. The proteins in the gel were transferred to 0.45 μm PVDF membranes. After treating with blocking buffer (5.0% (w/v) skimmed milk in PBS, 0.05% (v/v) Tween 20), the membrane was incubated with monoclonal antibody 3F4 at 4 °C overnight, then incubated with HRP-conjugated sheep anti-mouse IgG (Sigma-Aldrich Corp.). Bound antibody was visualized by chemiluminescence (ECL-Plus) on X-ray film. The titer of PrP^{Sc} present in the samples was calculated as described for method 1 in Section 2.2.1.

2.3. Evaluation of PrP^{Sc} removal by filtration

A 10% (v/v) concentration of "super-sonicated" 263K MF was prepared in PBS, and 10 ml aliquots were then filtered through a 220 nm or a 100 nm 4 cm^2 PVDF filter (Millex-GV or -VV, Millipore Corp.). In addition, 25 ml aliquots of "super-sonicated" 263K MF in PBS were filtered through a 0.01 m^2 P-75N (72 ± 2 nm), P-35N (35 ± 2 nm), or P-15N (15 ± 2 nm) filter (Asahi Kasei Medical Co., Ltd. Tokyo, Japan). Two independent batches of 263K MF were used. WB1 analysis of samples before and after filtration was performed to determine the removal of PrP^{Sc} under the different conditions. Non-sonicated 263K MF (from the same batch of 263K MF) was also filtered as a control.

2.4. Hamster bioassay to determine the infectious titer of 263K scrapie stocks

Three- to four-week-old female specific pathogen-free (SPF) Syrian hamsters were used in these experiments. Serial 10-fold dilutions of each sample or positive control were prepared in PBS. Six hamsters per sample dilution were inoculated intra-cerebrally with 0.02 ml per animal. The inoculated animals were monitored daily for general health, and weekly for clinical evidence of scrapie. Animals were euthanized once advanced signs of scrapie were evident, or at the end of the assay period (200 days). The brain was removed from each hamster following euthanasia: one half was fixed for histopathology and the other half was stored frozen at −70 °C for further analysis if required. For histopathological analysis, sections taken at four standard coronal levels, to cover the nine areas of the brain which are recognized to be mostly infected by the scrapie agent, were stained with hematoxylin and eosin, and scored for the presence or absence of scrapie lesions [15]. Histopathological analysis was performed on samples from around the clinical end-point of the titration assays, to confirm the clinical results. Hamsters that died during the